

1 Water chemistry and greenhouse gas concentrations in waterbodies of a thawing permafrost
2 peatland complex in northern Norway
3 Jacqueline K. Knutson¹, François Clayer¹, Peter Dörsch^{2,3}, Sebastian Westermann^{2,4}, Heleen
4 A. de Wit^{1,2}.
5 1 Norwegian Institute for Water Research, Økernveien 94, 0579, Oslo, Norway
6 2 Centre for Biogeochemistry in the Anthropocene, University of Oslo, Oslo, 0371, Norway
7 3 Faculty of Environmental Sciences and Natural Resource Management, Norwegian
8 University of Life Sciences (NMBU), 1433 Ås, Norway
9 4 Department of Geosciences, University of Oslo, Oslo, 0371, Norway
10
11 Correspondence: Jacqueline K. Knutson (jacqueline.knutson@niva.no)

12 1 Abstract

13 Thermokarst ponds in thawing permafrost landscapes play a considerable role in greenhouse
14 gas (GHG) emissions despite their small size, yet they remain underrepresented in Earth

15 [Transitions from hydrologically isolated thermokarst ponds in peat plateaus](#)

16 [to connected wetlands can substantially alter GHG dynamics. However, the processes and](#)

17 [GHG impacts of these, but the biogeochemical processes underlying these shifts are not well](#)

18 [understood, —particularly in the sporadic permafrost zones of Fennoscandia, where such](#)

19 [small systems are infrequently reported. To address this, we investigated At the Iškoras site in](#)

20 [northern Norway, a peat plateau with decaying permafrost and thermokarst ponds adjacent to](#)

21 [a wetland, we studied](#) water chemistry, dissolved organic matter (DOM) processing, and

22 GHG fluxes over two years [at the Iškoras site in northern Norway, where a degrading peat](#)

23 [plateau includes both thermokarst ponds and an adjacent wetland stream. Thermokarst ponds](#)

24 exhibited low pH, high organic acidity, and high oversaturation of dissolved carbon dioxide

25 (CO₂) and especially high dissolved methane (CH₄). Adjacent wetland streams, however,

26 with near-neutral pH, showed lower CH₄ and organic acidity but significantly higher CO₂

27 emissions despite moderate saturations driven by turbulence and bicarbonate replenishment.

28 By contrast, CO₂ emissions in ponds were primarily linked to DOM mineralization. [Despite](#)

29 [differences in chemistry, DOM mineralization rates were similar between ponds and streams,](#)

30 suggesting that environmental factors like pH and microbial community differences

31 counteract DOM lability variations. As permafrost decays and transitions from peat plateaus

32 to wetlands, ponds as hotspots of CH₄ emissions will disappear. However, total GHG fluxes

33 across the peatland-wetland continuum will depend on wetland emissions, where CH₄

34 emissions usually are considerable, and the fate of organic matter within the plateau. Lateral

35 DOM fluxes may represent a significant loss of soil organic carbon, highlighting the

36 importance of hydrological connectivity in linking terrestrial and aquatic systems. This study

37 emphasizes the need to account for the relationship between hydrological and chemical
38 processes when assessing C and GHG fluxes in permafrost-impacted regions.

39 1. Introduction

40 Northern latitude [permafrost](#) regions [hold one of the largest terrestrial carbon reservoirs on](#)
41 [the planet \(Schuur et al., 2008; Schuur et al., 2015; Walter et al., 2006\)](#). Although covering
42 [only about 15% of global soils, these regions store an estimated 1400-1600 Pg of organic](#)
43 [carbon \(OC\) \(Hugelius et al., 2014; Schuur et al., 2022; Strauss et al., 2025\)](#), making them a
44 [critical component of the global carbon \(C\) cycle, which store approximately 1,300 Pg of](#)
45 [organic carbon \(OC\) \(Hugelius et al., 2014\)](#), represent one of the largest terrestrial carbon
46 [reservoirs on Earth \(Schuur et al., 2008; Schuur et al., 2015; Walter et al., 2006\)](#). Sequestered
47 under cold and oxygen-limited conditions, this [carbon \(C\)C](#) is increasingly vulnerable to
48 release as permafrost thaws due to climate warming, generating significant feedbacks that
49 complicate predictions of future climate trajectories (Schuur et al., 2008; Schuur et al., 2015;
50 Walter et al., 2006). As permafrost degrades, the release of greenhouse gases, particularly
51 methane (CH_4) and carbon dioxide (CO_2), through the microbial decomposition of previously
52 frozen organic matter (OM) can rapidly escalate the impact of this feedback (Schuur et al.,
53 2008; Walter et al., 2008; Wik et al., 2016; Zimov et al., 2006). While the large-scale thaw of
54 permafrost is widely recognized (Leppiniemi et al., 2023) [and permafrost regions warm three](#)
55 [to four times faster than the global average \(Meredith et al., 2019\)](#), the timing, magnitude,
56 and pathways of carbon release remain uncertain, influenced by processes such as burial,
57 mobilization, lateral export, and mineralization (Verdonen et al., 2023; Vonk et al., 2015).

58 Permafrost thaw leads to irreversible landscape transformations. Peatlands in northern
59 Norway are predominantly located in the sporadic permafrost zone, where they form
60 distinctive landscape features such as peat plateaus and palsas. These are peat uplands and
61 mounds with a frozen core, elevated above the water table by the formation of segregation ice
62 (Alewell et al., 2011; Krüger et al., 2017). As these features degrade, permafrost thaw is often
63 abrupt and subsidence and collapse is to be expected, leading to the formation [of](#) thermokarst

64 ponds, as excess ground ice is lost (Martin et al., 2021). More than half of the permafrost
65 areas in the Scandinavian Peninsula are at risk of disappearing under current and projected
66 climate conditions (Gisnås et al., 2017; Schuur et al., 2008). The areal extent of peat plateaus
67 in this region decreased by 33%–71% between the 1950s and the 2010s, with rapid
68 degradation observed during the last decade (Borge et al., 2017). This regional degradation
69 mirrors processes observed across the northern hemisphere, including in the Canadian Arctic,
70 European Russia, and the Kola Peninsula, highlighting the vulnerability of sporadic
71 permafrost regions to warming climates (Krutskikh et al., 2023; Payette et al., 2004; Sannel
72 and Kuhry, 2011). While the processes driving [these permafrost thaw and landscape](#)
73 transformations, such as thermal disturbances, vegetation shifts, and subsidence, are
74 relatively well-studied, their consequences for GHG fluxes and C cycling remain uncertain,
75 limiting our ability to project future climate feedbacks (Holmes et al., 2022; Olefeldt et al.,
76 2021; Turetsky et al., 2020).

77 Among the new landscape forms that emerge from degrading peat plateaus, thermokarst
78 ponds and wetlands play a critical role in greenhouse gas dynamics. These small aquatic
79 systems, formed by the thaw and collapse of permafrost, are characterized by high
80 concentrations of dissolved organic carbon (DOC) and inorganic carbon (DIC) (Abnizova et
81 al., 2012; Martin et al., 2021; Matveev et al., 2018). Thermokarst ponds, in particular, act as
82 hotspots for CH₄ and CO₂ emissions due to unique biogeochemical conditions, including
83 hydrological isolation, anoxic sediments, and high organic matter availability (in 't Zandt et
84 al., 2020; Polishchuk et al., 2018; Vonk et al., 2015; Ward and Cory, 2015). Despite [their the](#)
85 small size [of thermokarst ponds](#), these waterbodies can contribute significantly to regional C
86 fluxes, with CH₄ and CO₂ supersaturation levels often surpassing those of larger lakes [—](#)
87 [whether thermokarst or not](#) [—](#) or surrounding tundra ecosystems (Abnizova et al., 2012; Kuhn
88 et al., 2018; Shirokova et al., 2012). However, [their the](#) contributions [of thermokarst ponds](#)

89 are often overlooked in large-scale C assessments, as they remain difficult to detect using
90 satellite-based methods because of their small size (Holgerson and Raymond, 2016; Muster et
91 al., 2017).

92 As permafrost thaw progresses, the transition of isolated thermokarst ponds to interconnected
93 wetland systems further alters GHG dynamics. While northern permafrost wetlands currently
94 act as a C sink, the inclusion of thaw pond emissions into broader wetland carbon budgets
95 reveals their potential to offset the sink capacity by 39% (Kuhn et al., 2018). Compared to
96 thermokarst ponds, wetlands have sustained CH₄ fluxes over larger areas due to persistent
97 waterlogging and OM decomposition (Pirk et al., 2024; Swindles et al., 2015; Turetsky et al.,
98 2020), thus constituting important long term CH₄ sources (Bansal et al., 2023). The
99 transformation from stable permafrost to thermokarst landscapes is accompanied by shifts in
100 hydrology, OM lability, and microbial activity, which collectively shape CO₂ and CH₄
101 production pathways (Holmes et al., 2022; Laurion et al., 2020). Understanding the dynamics
102 of these evolving [permafrost and wetland](#) systems is critical for assessing the broader impacts
103 of permafrost thaw on regional C uptake and emissions as well as global C cycles.

104 Northern Norway's sporadic permafrost zone, with its abundant small thermokarst ponds and
105 emerging wetlands, provides a valuable opportunity to [investigate carbon cycling in rapidly](#)
106 [evolving subarctic landscapes](#)~~study such processes~~. The region's [rapidly](#)-degrading peat
107 plateaus host significant C stocks, yet small aquatic systems, especially those in
108 Fennoscandia, remain underrepresented in Earth system models (Abnizova et al., 2012;
109 Muster et al., 2019; Muster et al., 2017). [While](#) ~~E~~xisting studies emphasize the importance
110 of quantifying CH₄ and CO₂ fluxes in these environments and their implications for C
111 budgets (Abnizova et al., 2012; Matveev et al., 2018). [However, the interactions between](#)
112 [hydrology, vegetation and carbon processing are not well understood. Yet such processes are](#)
113 [central to key questions regarding how transitions between permafrost, thermokarst, and](#)

114 wetland systems influence C dynamics, and whether these landscapes function as net C
115 sources or sinks under changing climatic conditions (Sim et al., 2021). In particular, peatland
116 ponds and thermokarst waterbodies exhibit unique biogeochemical cycling from lakes, driven
117 more by internal dynamics than external watershed inputs (Arsenault et al., 2022). These
118 differences remain poorly represented in both observational datasets and Earth system
119 models.yet will control critical questions remain regarding how transitions between
120 permafrost, thermokarst, and wetland systems influence C dynamics, and whether these
121 landscapes function as net C sources or sinks under changing climatic conditions (Sim et al.,
122 2021).

123 This study aims to address these gaps by examining the GHG dynamics and C
124 biogeochemistry of thermokarst ponds and wetland streams in the sporadic permafrost zone
125 of northern Norway. Over two years, we collected a novel dataset combining biogeochemical
126 measurements with C flux data from thermokarst ponds and a wetland stream within a small
127 permafrost peatland plateau undergoing rapid permafrost degradation. This setting captures a
128 landscape in active transition from isolated thermokarst ponds to interconnected wetlands.we
129 measured dissolved CO₂ and CH₄ concentrations, water chemistry, and OM lability to
130 evaluate the processes driving C fluxes in these systems. We hypothesize that (1) thermokarst
131 ponds serve as hotspots of CH₄ and CO₂ production relative to wetland streams, (2) the
132 transition from isolated ponds to wetlands significantly alters GHG emission pathways,
133 driven by shifts in hydrology and OC availability, and (3) recently mobilized OM from
134 thawing permafrost presents a labile source of C promoting CO₂ production in thermokarst
135 water bodies compared to wetland streams. By exploring these dynamics, this study provides
136 insights into the role of small water bodies in permafrost C feedbacks, advancing our
137 understanding of sub-Arctic and boreal C cycling.

138 2. Methods

139 2.1 Study area

140 The Iškoras field site (69.34°N, 25.29°E; 381 m a.s.l.) is a permafrost peatland plateau
141 located in the interior of the Finnmark province, northern Norway, on the Finnmarksvidda
142 plateau (Fig. 1). The region of Finnmarksvidda lies between 300 and 500 m a.s.l. and is
143 characterized by a subarctic continental climate. The topography was shaped by Pleistocene
144 glaciations, which deposited ground moraines, glaciofluvial, and glaciolacustrine sediments
145 (Sollid et al., 1973). The depressions in the landscape are commonly filled with peatlands
146 (Borge et al., 2017), and peat plateaus underlain by permafrost are common.

147 The Iškoras peat plateau covers an area of approximately 4 ha and is part of a 3.3 km²
148 subarctic headwater catchment that drains into the Bákiljohka river (91 km²). Mean annual
149 air temperature and precipitation for the 30-year normal (1991-2020) period was -1.9°C ±
150 1.0°C, and 513 ± 90 mm, respectively (Table 1). For our study period 2021 to 2022, MAAT
151 and MAP were -1.1°C, and 589.5 mm (SeNorge, 2023). Iškoras lies within the zone of
152 sporadic permafrost and the peat soils extend down to about 1.5 m in the plateau areas
153 (Kjellman et al., 2018) and active layers depths up to 90 cm. The plateau exhibits a complex
154 surface of intact and degrading palsas, along with thermokarst ponds, and is surrounded by
155 wetlands and a stream to the northwest (Martin et al., 2019). Between 2019 and 2022, up to
156 0.8 m of subsidence of palsas was measured at localized sites (Pirk et al., 2024). The site is
157 located about 90 km south of the nearest coastal fjord and is dominated by mountain birch
158 forest (*Betula pubescens*) and tundra vegetation, including dwarf birch (*B. nana*). The plateau
159 consists primarily of low heath shrubs, Ericaceae (*Empetrum nigrum*, *Rhododendron*
160 *tomentosum*), lichen crusts, mosses, and cloudberry (*Rubus chamaemorus*) or bare ground,
161 while the surrounding wetlands are dominated by Sphagnum mosses, sedges (*Carex* spp.),
162 and cotton grass (*Eriophorum* spp.) (Kjellman et al., 2018; Martin et al., 2019).

	Unit	Mean ± std for 1991-2020	Mean + std for 2021-2022
annual temperature	°C	-1.9 ± 1.0	-1.1 ± 0.4
summer temperature	°C	10.4 ± 2.2	11.8 ± 0.2
annual precipitation	mm	513 ± 90	589.5 ± 62.5
summer precipitation	mm	196 ± 53	207 ± 48

Table 1 Mean and interannual standard deviation (shown as mean ± std) of climate parameters

for the Iškoras catchment for the normal period (1991–2020) and the study period 2021-2022.

Summer is defined as May to September.

166

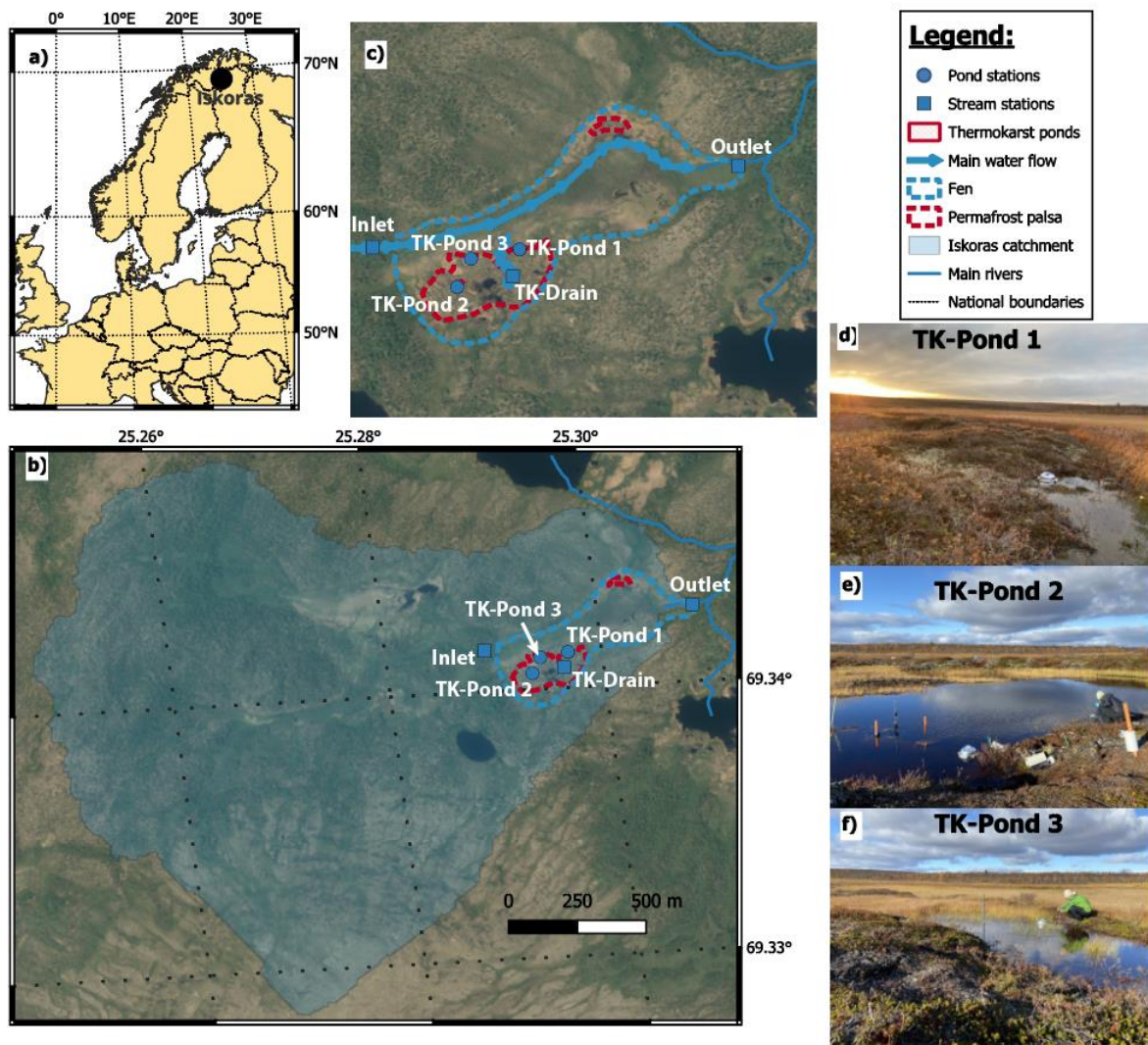
167 The study area included water bodies within a peat plateau and the adjacent wetland, selected
 168 for sampling and monitoring. Measurements and samples were taken approximately monthly
 169 in the ice-free season from May until October in 2021 and 2022 ([full details in Table SI 1](#)).

170 The waterbodies consisted of three thermokarst ponds (TK-Pond 1, 2, and 3), a seasonal
 171 drainage channel (TK-Drain) connecting the peat plateau to the wetland, and the wetland's
 172 inlet and outlet streams (Inlet, Outlet), with the outlet also marking the terminus of the
 173 Iškoras catchment. From mid-May to early November, monitoring showed that the
 174 thermokarst ponds and Inlet were ice-free for 170 ± 5 days, while the Outlet remained ice-
 175 free for 184 days (Table SI [24](#)).

176 The thermokarst ponds varied in hydrological connectivity and permafrost influence,
 177 reflecting differences in age and physical characteristics. TK-Pond 1 (0.4 m depth) is small
 178 and located at the peat plateau–wetland transition, experiencing periodic hydrological
 179 isolation. TK-Pond 2, the largest and deepest (1.5 m depth), lies centrally on the peat plateau,
 180 surrounded by degrading palsas. TK-Pond 3 (0.6 m depth) is situated at the plateau's edge and
 181 was initially isolated by a surrounding permafrost mound.

182 The TK-Drain is a shallow, ephemeral drainage channel that provides the primary
 183 hydrological connection between the peat plateau and wetland. The wetland's inlet stream
 184 (0.6 m wide, 15–40 cm deep) begins approximately 200 m upstream of the plateau, flowing
 185 through birch forest and mires without permafrost before entering the wetland where the

186 channel becomes less defined. The outlet stream (0.8 m wide, 30–60 cm deep) re-emerges
187 approximately 700 m downstream at the wetland's far end, serving as the catchment outlet.
188 Between September 2020 and October 2022, a total of nine field campaigns were conducted
189 for regular sampling of water chemistry, dissolved gases, CO₂ emissions, [GHG production](#)
190 [using the](#) dark incubations [method](#), and high-frequency monitoring of water height and
191 temperature.



192

193 **Figure 1 Location map** of the study area in Europe (a) and the Iškoras catchment (b; determined
194 from the outlet station Outlet). Close-up of the wetland (c) with regular sampling sites and main water
195 flow direction. Pictures of the three main pond sites are also shown (d–f).

196 2.2 Water chemistry

197 Water samples for chemical analyses were collected using standardized procedures. From
198 each site, 500 mL unfiltered water was collected in HDPE rectangular bottles (Emballator
199 Melledrud AB, Stockholm, Sweden) after rinsing with sample waters three times, kept dark
200 after sampling, carried out of the field, and stored within hours after sampling at 4°C. The
201 samples were then transported by car and plane back to the laboratory and delivered for
202 chemical analysis where they were kept at 4°C until analysis. To ensure that our sampling
203 procedures were suitable for the determination of nutrient concentrations, we performed a
204 comparison of different field procedures including acidification and filtration in the field (see
205 Supplementary information). We found no significant differences between procedures (Table
206 SI 4). Chemical analysis of pH, electrical conductivity (EC), alkalinity, and concentrations of
207 sulfate (SO_4^{2-}), silica (SiO_2), ammonium (NH_4^+), nitrate (NO_3^-), total phosphorous (totP),
208 total organic carbon (TOC), DOC (filtered by 0.45 μm) and particulate organic carbon (POC)
209 (filtered and then combusted at 1800 °C) in the water samples was performed at accredited
210 laboratories at the Norwegian Institute for Water Research (NIVA); methods for analysis and
211 quality control are described in Vogt and Skancke (2022 the ICP Waters Programme Manual
212 (Gunderson et al., 2025). The samples were not fully digested according to standard
213 procedures required for the determination of total nitrogen (totN), hence totN values are
214 expected to be underestimated and are therefore not shown in the manuscript, although the
215 values were enough to confirm the dominant form of N was organic (Thrane et al., 2020)
216 totN values were enough to confirm that the dominant form of N was organic..
217 Absorption spectra of DOM were measured at NIVA for wavelengths between 200 and 900
218 nm, using 1 nm intervals, with a 5 cm cuvette length and Milli-Q water as a reference, using a
219 Lambda 40 UV/Vis spectrophotometer (Perkin Elmer, USA) and expressed in absorbance pr
220 cm. In two samples, incomplete filtration caused excess scattering, and these spectra were

221 removed. The absorbance values at 254 nm ($A_{\lambda 254\text{nm}}$) were used to calculate specific UV
222 absorbance, expressed as sUVa~~The absorbencies were used to calculate specific UV~~
223 absorbency (sUVa = $A_{\lambda 254\text{nm}}/\text{mg C L}^{-1}$) and the specific UV absorption ratio (SAR =
224 $A_{\lambda 254\text{nm}}/A_{\lambda 400\text{nm}}$) was calculated for each sample.

225

226 2.3 Dissolved gas analysis

227 Dissolved gases (CO₂, CH₄) were sampled in the field using the acidified headspace
228 technique (Åberg and Wallin, 2014). Duplicate gas samples were collected according to
229 Valiente et al. (2022)- with Two-50 mL syringes. These were filled and sealed underwater
230 without air bubbles to prevent gas loss. Excess water was expelled to retain 30 mL, and 20
231 mL of ambient air was drawn in to create a headspace. All sSamples were acidified with 0.6
232 mL of 3% HCl to achieve pH <2, ensuring DIC was present as CO₂. Equilibrium was reached
233 by shaking for one minute, followed by a 30-second rest, repeated thrice and then 15 mL of
234 headspace gas was transferred to 12 mL evacuated vials., and wWater temperature in the
235 syringe was measured immediately after gas transfer. Samples were stored at room
236 temperature and flown to southern Norway for analysis. A 15 mL ambient air sample was
237 taken daily for background correction.

238 Analysis was performed via automated gas chromatography (GC) at the Norwegian
239 University of Life Sciences (NMBU), as described by Yang et al. (2015). A GC autosampler
240 (GC-Pal, CTC, Switzerland) injected 2 mL headspace samples into an Agilent 7890A GC
241 (Santa Clara, CA, USA) with a 20-m wide-bore Poraplot Q column at 38°C, using He as the
242 carrier gas to separate CH₄ and CO₂ from Ar, N₂, and O₂. For calibration, certified standards
243 of CO₂ and CH₄ in He were used (AGA, Germany) and N₂, O₂, and Ar were calibrated using
244 laboratory air. CH₄ was measured with a flame ionization detector (FID). A thermal
245 conductivity detector (TCD) was used to measure all other gases.

246 Dissolved gas concentrations were calculated from headspace concentrations corrected for
247 background air, applying temperature-adjusted Henry's law constants (Wilhelm et al., 1977)
248 based on the recorded water temperature. At pH >4, a non-negligible amount of DIC is in the
249 form of (bi)carbonates (HCO_3^- , CO_3^{2-}). The bicarbonate concentrations were calculated based
250 on pH, total dissolved CO_2 (after acidification), and the temperature-adjusted first
251 dissociation constant ($\text{pK}_1 = 6.41$ at 25°C ; Stumm and Morgan (2013)) of the carbonic acid
252 equilibrium. Dissolved CO_2 was calculated as DIC minus bicarbonate. To facilitate
253 comparisons with existing studies that report dissolved gases in μatm , we converted dissolved
254 gas concentrations to CO_2 or CH_4 saturation indexes (GHG_{SI}) assuming atmospheric partial
255 pressures of CO_2 and CH_4 as 400 μatm and 1.9 μatm , respectively:

$$256 \quad GHG_{SI} = \frac{[GHG]}{[GHG]_{saturation}}$$

257 Where $[GHG]$ is the measured dissolved CO_2 or CH_4 concentration, and $[GHG]_{saturation}$ is
258 the concentration of dissolved CO_2 or CH_4 at equilibrium with their respective atmospheric
259 partial pressure.

260

261 2.4 Diffusive CO_2 fluxes from water to atmosphere

262 Measurements of CO_2 fluxes from water to atmosphere (diffusive CO_2 fluxes) were measured
263 at each site for 30-60 minutes using self-made, opaque flux chambers as described by
264 Bastviken et al. (2015) at the water-air interface. The chamber consists of a Senseair K30
265 sensor (Senseair AB, Delsbo, Sweden) housed within a plastic bucket that records pCO_2 ,
266 temperature, and relative humidity every 30 seconds. Fluxes are calculated from the linear
267 increase in pCO_2 corrected for ambient temperature and humidity in the chamber (Bastviken
268 et al., 2015) considering the internal air volume and the water surface area covered by the
269 chamber. Single measurements with a linear increase in pCO_2 with time associated with a
270 coefficient of determination (R^2) lower than 0.9 were discarded.

271

272 2.5 Dark incubations

273 Water samples were collected for short term dark incubations started directly in the field
274 lasting between 18 and 30 hours to estimate DOM mineralization and GHG production
275 processing rates. Serum flasks (120 mL) were filled with 80 mL of water with a 50 mL
276 syringe equipped with a long tube. The syringe was filled and closed under water, and the
277 water was gently pushed at the bottom of the serum flask to prevent gas loss. The remaining
278 40 mL were left with ambient air as headspace. The flasks were crimp-sealed with gas-tight,
279 butyl-rubber septa, sealed, covered with aluminium foil and kept at field temperature (for
280 maximum 6 hours), transported back from the field to be stored at room temperature (18-
281 20°C). The day following the sampling (18 to 30 hours after sampling), the incubations were
282 stopped by adding 1.6 mL 3% HCl to reach a final pH below 2, after which gas samples were
283 taken following the protocols described above. Results from the dark incubation were
284 expressed as rates of DIC production over the course of the incubation period by comparison
285 with initial DIC concentrations and reported as μMh^{-1} :

286
$$\text{DIC}_{\text{rate}} = \frac{[\text{DIC}]_f - [\text{DIC}]_0}{h} \quad (\text{Eq. 2})$$

287 where $[\text{DIC}]_f$ is the final solute concentrations in the dark incubation and $[\text{DIC}]_0$ is the initial
288 solute concentration taken in the field (see Sect 2.3) in μM , and h is the incubation duration
289 in hours. In addition, we normalized the DIC production rate with DOC concentration to
290 estimate DOM mineralization rates (per time unit). Also, we calculated the first-order DOM
291 decay rate (yr^{-1}) using the exponential decay rate model (Mostovaya et al., 2017). The
292 exponential decay model, based on early studies on sediment diagenesis (Boudreau and
293 Ruddick, 1991; Westrich and Berner, 1984), is often the best model to describe decay rates
294 from bioassays in closed systems (Vähätalo et al., 2010) and has been widely used to describe

295 DOM degradation reactions. Under the exponential decay model, the decay constant (k_{DOM} ;
296 yr^{-1}) can be expressed as:

297
$$k_{DOM} = \ln \left(\frac{DOC}{DOC - ([DIC]_f - [DIC]_0)M_C} \right) \times \frac{8766}{h} \quad (\text{Eq. 3})$$

298 where DOC is the DOC concentration in $\mu\text{g L}^{-1}$, M_C is the molecular mass of C in g mol^{-1} and
299 8766 is the number of hours in a year. Where $[DIC]_f$ was equal to or below $[DIC]_0$, we
300 removed the values from the dataset assuming that the temperature correction of $[DIC]_0$ was
301 not precise enough (three of 39 samples) to allow quantification of CO_2 processing rates.
302 These occurred in September 2020 and October 2021, under cold field conditions, when
303 $[DIC]_0$ was overestimated because of unknown sample temperature in the field.

304

305 2.6 Statistical methods

306 Statistical analyses were conducted to evaluate differences between sites for various
307 measured parameters. One-way analysis of variance (ANOVA) was employed to test for
308 differences among groups. Pairwise comparisons of group means were performed using
309 Student's t-test using JMP 18.0.11 (2024 JMP Statistical Discovery LLC). For data that did
310 not conform to normal distribution assumptions, non-parametric methods were applied,
311 specifically the Wilcoxon rank-sum test, to ensure robust comparisons across sites. Results
312 are displayed in the form of connecting letters reports within the tables. Sites with the same
313 letter (e.g., "A" or "B") indicate no statistically significant differences in the measured
314 parameter between those groups at the $p < 0.05$ significance level. Groups with different
315 letters (e.g., "A" vs. "B") are significantly different. When overlapping letters (e.g., "AB") are
316 reported, those groups are statistically similar to others with at least one shared letter but may
317 differ from groups with entirely distinct letters. Figures were created using the ggplot2
318 package (Wickham, 2016) using R software (R Core Team, 2021).

319 3. Results

320 3.1 Water chemistry

321 The thermokarst water bodies were more acidic, richer in DOC and total P, and lower in
322 SO_4^{2-} and SiO_2 compared with the wetland streams (all differences statistically significant;
323 Table 2; Fig. 2). The low pH of the ponds is consistent with their high DOC, and thus high
324 organic acidity. The water bodies aligned along the inverse DOC-pH relationship with TK-
325 Pond 3 exhibiting the highest DOC and lowest pH at the top, followed by TK-Pond 2 and TK-
326 Pond 1. The TK-Drain usually held an intermediate position between the thermokarst ponds
327 and the wetland streams, which were found at the high pH – low DOC end of the DOC-pH
328 relationship curve. Similar patterns were found for DOC- SO_4^{2-} and DOC- SiO_2 relationships
329 (Fig. 2). Particulate OC concentrations were significantly higher and more variable in
330 thermokarst ponds ($1.2\text{--}3.4 \text{ mg L}^{-1}$) compared to wetland streams ($0.4\text{--}0.6 \text{ mg L}^{-1}$), with
331 greater variability observed at the Outlets than Inlet (Table 2). ~~was on average <5% of TOC in~~
332 ~~the wetland streams, while POC showed considerably more variation in the thermokarst~~
333 ~~water bodies, possibly related to inputs from destabilized organic matter from the thawing~~
334 ~~permafrost.~~

335 All water bodies had NO_3^- concentrations at, or close to, the detection limit, while the
336 thermokarst water bodies had considerable levels of NH_4^+ contrary to the wetland streams
337 (Table 2). Total P was highest, and most variable, in the ponds which to some extent mirrored
338 the pattern in DOC, understandably given that in these nutrient-poor sites most P would be in
339 an organic form just like N. Despite incomplete digestion, totN values were enough to
340 confirm that the dominant form of N was organic.

341 The DOM quality indicator SAR was highest in the thermokarst ponds ($p<0.03$). SAR was
342 positively strongly correlated with DOC concentration (positive, $R^2 0.57$, $p<0.0001$),
343 implying that lowest SAR was found in the wetland streams. The Other DOM quality

344 indicators (sUVA, ~~associated with a proxy for aromaticity~~) was slightly tended to be
 345 somewhat higher in the wetland streams than in the thermokarst ponds, although the
 346 difference was not significant but did not show significant differences between wetlands and
 347 thermokarst water bodies.

348

349 **Table 2. Water chemistry parameters for thermokarst ponds and wetland sites during nine**
 350 **sampling campaign.** Median values with standard deviations are shown for all water chemistry
 351 variables, except for pH, which is shown as the median with minimum and maximum values. EC:
 352 electrical conductivity; SO₄²⁻: Sulfate; SiO₂: silica; DOC: dissolved organic carbon; sUVA: specific
 353 UV absorbency, SAR: specific UV absorption ratio; TOC: total organic carbon; NH₄⁺: ammonium;
 354 NO₃⁻: nitrate, totP: total organic phosphorous; POC: particulate organic carbon (POC, % of TOC).
 355 Letters indicate significant differences between sites for each variable (Tukey's *t*-test, pairwise
 356 comparisons, *p*<0.05; see Sect. 2.6).

	pH	EC mS m ⁻¹	SO ₄ ²⁻ mg SO ₄ ²⁻ L ⁻¹		SiO ₂ mg SiO ₂ L ⁻¹			
			B	C	BC	C		
TK-Pond 1	4.49 (4.16-4.79)	B	2.1 (0.7)	B	0.12 (0.07)	C	2.4 (1.8)	BC
TK-Pond 2	4.23 (4.03-4.37)	C	3.2 (0.7)	A	0.18 (0.20)	C	1.0 (1.0)	C
TK-Pond 3	4.06 (3.79-4.32)	C	4.0 (1.6)	A	0.11 (0.02)	C	4.3 (1.7)	B
TK-Drain	4.79 (4.63-4.88)	B	1.6 (0.1)	B	0.16 (0.08)	C	2.3 (1.9)	BC
Inlet	6.69 (6.11-7.36)	A	2.0 (0.5)	B	0.85 (0.18)	A	8.7 (2.4)	A
Outlet	6.56 (6.04-6.97)	A	1.9 (0.3)	B	0.60 (0.25)	B	8.6 (3.0)	A

	DOC mg C L ⁻¹	sUVA A _{λ254nm} /mg C L ⁻¹	SAR		TOC mg C L ⁻¹			
			ABC	A _{λ254nm} /A _{λ400nm}	BC	20.8 (5.1)	C	
TK-Pond 1	19.2 (4.4)	C	3.9 (0.4)	ABC	8.4 (0.3)	BC	20.8 (5.1)	C
TK-Pond 2	25.7 (6.4)	B	4.2 (0.3)	A	8.8 (0.5)	AB	27.4 (7.7)	B
TK-Pond 3	34.1 (6.8)	A	3.6 (0.6)	BC	9.2 (0.7)	A	34.8 (9.4)	A
TK-Drain	17.3 (6.6)	C	3.8 (0.4)	C	8.1 (0.2)	AB	19.5 (4.5)	C
Inlet	8.5 (2.1)	D	4.1 (0.4)	AB	7.6 (0.2)	C	8.4 (1.6)	D
Outlet	9.0 (1.5)	D	4.3 (0.3)	A	7.8 (0.2)	C	9.4 (1.6)	D

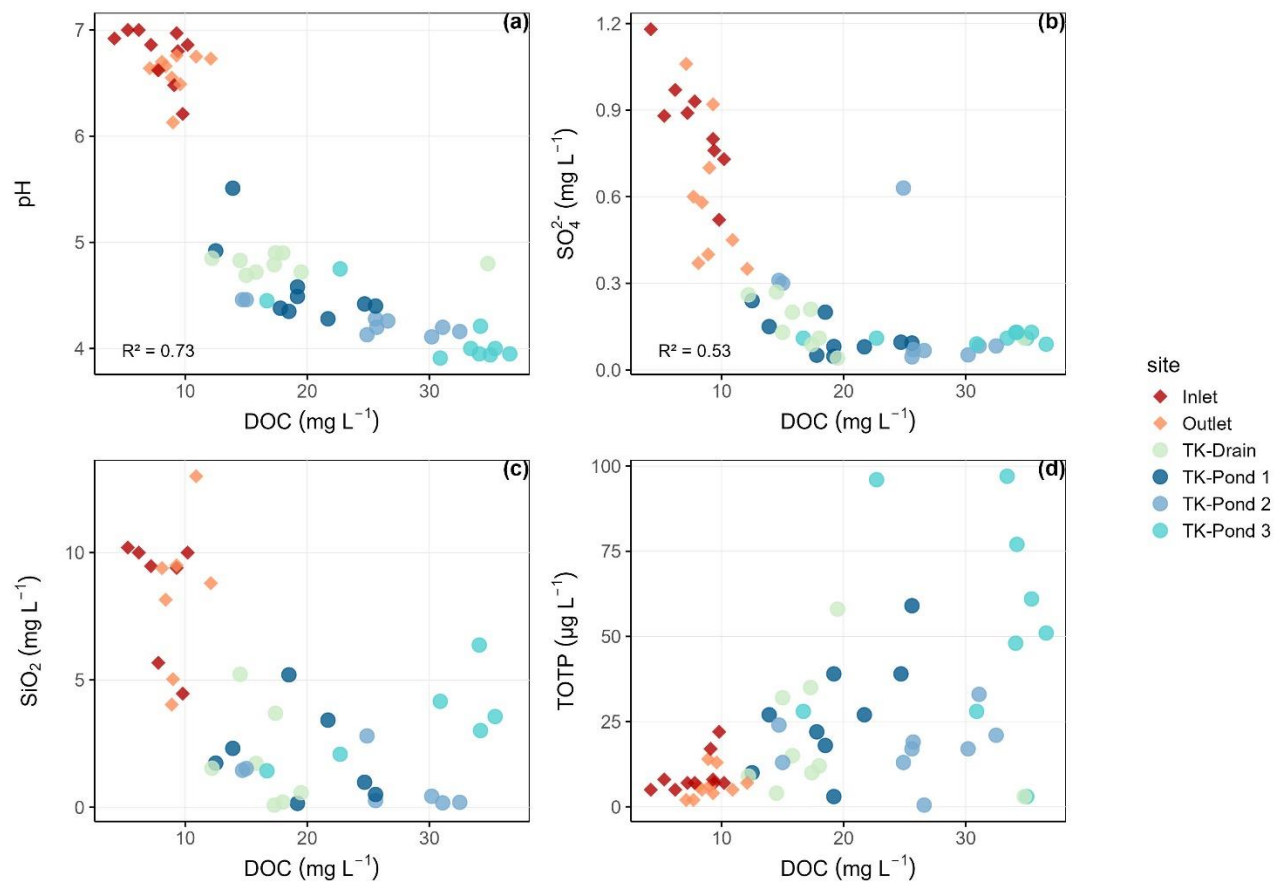
	NH ₄ ⁺ μg N L ⁻¹	NO ₃ ⁻ μg N L ⁻¹	TotP μg P L ⁻¹		POC mg C L ⁻¹			
			A	B	BC	1.2 (0.8)	B	
TK-Pond 1	23 (26)	B	2.0 (0.0)	A	27 (17)	B	1.2 (0.8)	B
TK-Pond 2	94 (105)	A	2.1 (0.3)	A	18 (9)	BC	1.8 (1.2)	A
TK-Pond 3	38 (77)	AB	1.9 (0.3)	A	54 (32)	A	3.4 (2.8)	A
TK-Drain	33 (20)	B	2.0 (0.0)	A	20 (18)	BC	3.3 (2.4)	A

Inlet	2 (2)	B	1.9 (0.3)	A	9 (6)	C	0.4 (0.2)	C
Outlet	4 (8)	B	1.9 (0.3)	A	7 (4)	C	0.6 (0.6)	C

357

358 The inverse relationship between DOC and pH points towards organic acidity as a strong
359 driver of pH. Additionally, the near-to-neutral pH in the wetland streams is consistent with
360 groundwater influences from the catchment, which also would explain as well as the elevated
361 SiO₂ and SO₄²⁻ concentrations. A limited set of water samples were analysed for base cations
362 (Table SI 43), confirming that these were highest in the wetland streams.

363 The water chemical composition of the ponds mirrored the impact of thawing permafrost: the
364 TK-Pond 3 is hydrologically most isolated with the lowest pH, highest conductivity, and
365 highest DOC. TK-Pond 1, located at the transition from peat plateau to wetland, had a higher
366 pH and lower EC, DOC and NH₄⁺ than the other ponds, which is consistent with some
367 hydrological influences from the wetland and hence less permafrost impact. TK-Pond 2 is
368 located in the middle of the peat plateau and is by far the largest pond and, under wet
369 conditions, hydrologically connected to neighbouring ponds. The water chemistry of TK-
370 Drain was usually most similar to that of TK-Pond 1. An example of pH and EC gradients
371 from the peat plateau into the wetland is consistent with the influence of thermokarst
372 waterbodies gradually becoming less dominant in the transition from the peat plateau
373 complex to the wetland (Fig. SI1).



374

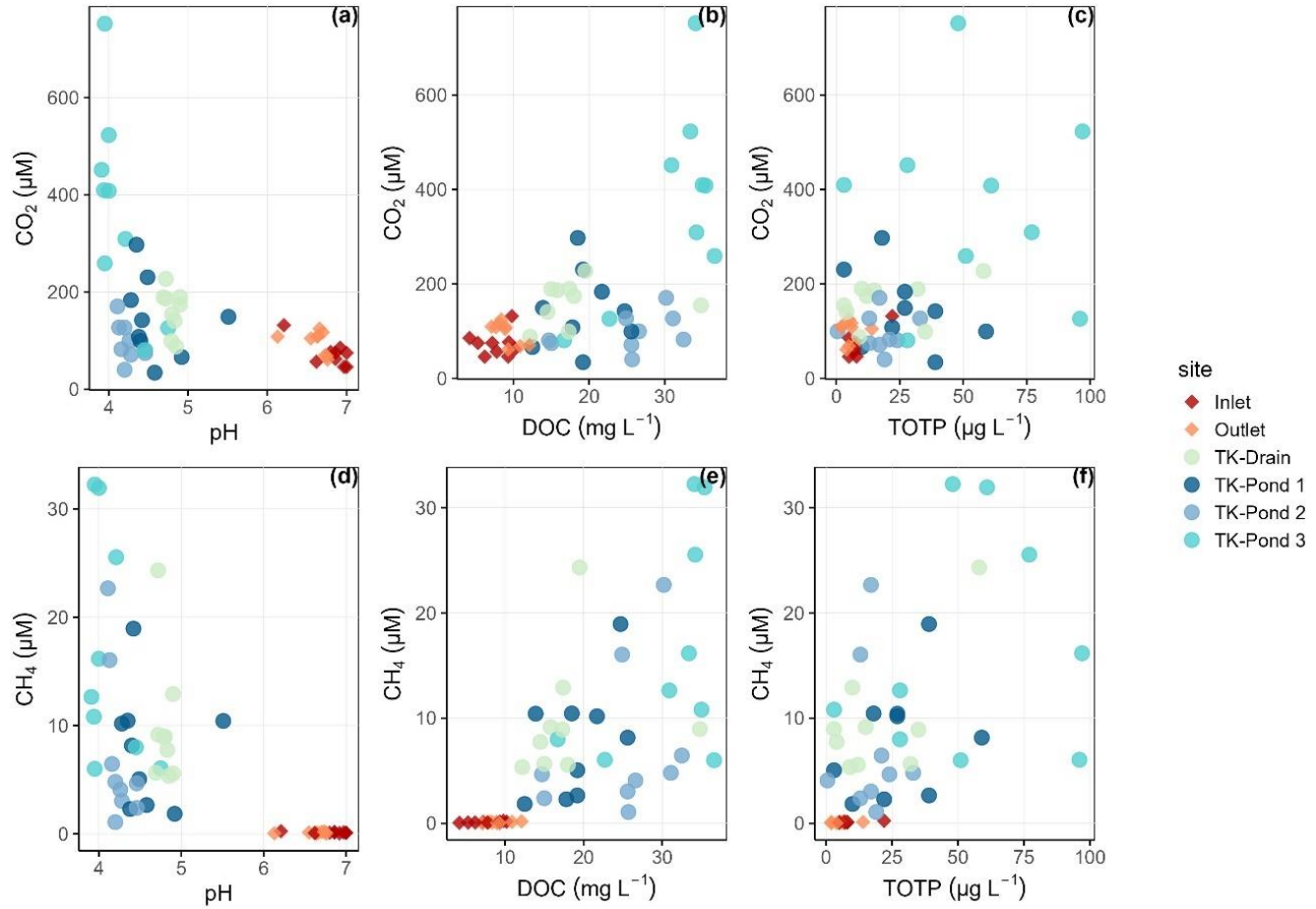
375 **Figure 2. Relationships between Dissolved Organic Carbon (DOC) and various water quality**
 376 **parameters across different sites.** The scatter plots demonstrate the relationships between dissolved
 377 organic carbon (DOC) and pH (a), sulfate (SO_4^{2-}) (b), silica (SiO_2) (c), and total organic phosphorus
 378 (totP) (d).

379

380 3.2 Dissolved gases and gas evasion

381 All water bodies were oxygenated and dissolved O_2 concentrations were on average 61 to
 382 81% of water O_2 saturation (Table 3). The ponds are shallow which allow for wind mixing
 383 and they host sphagnum, suggesting active O_2 production through photosynthesis. All water
 384 bodies were oversaturated with CH_4 and CO_2 . Dissolved CH_4 concentrations were 2000–5000
 385 and ~30 times higher than atmospheric equilibrium, in the ponds and in the wetland streams,
 386 respectively, indicating that all water bodies – thermokarst ponds in particular - are net

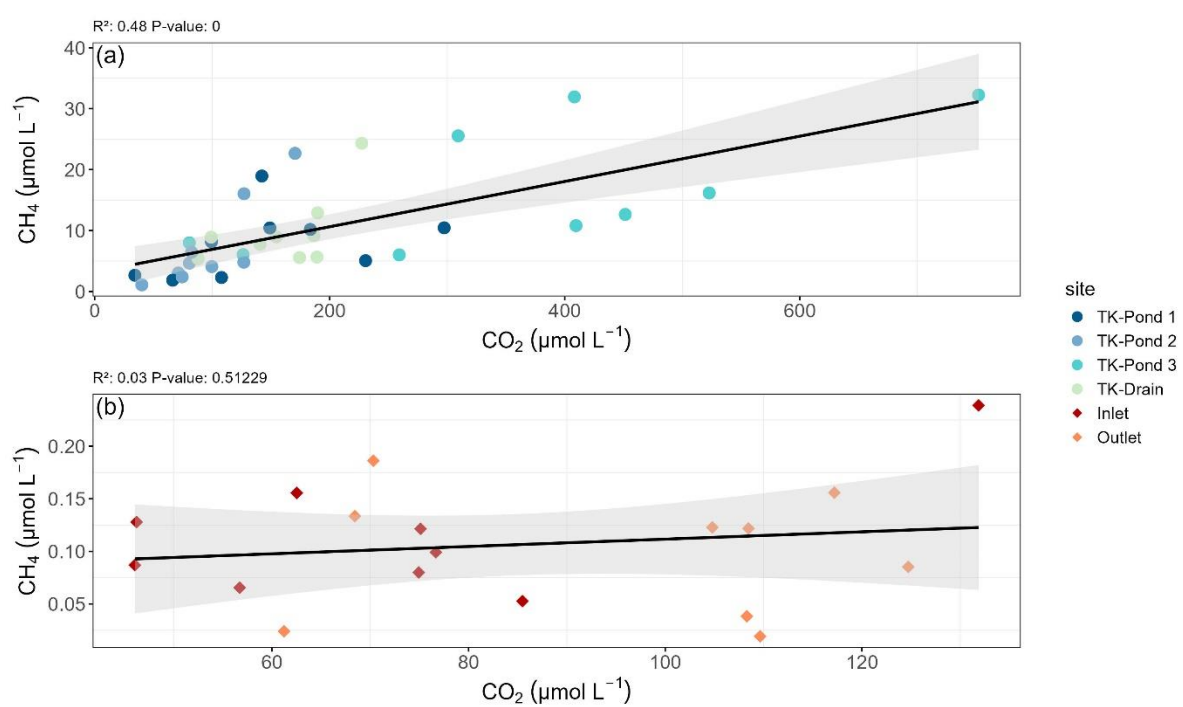
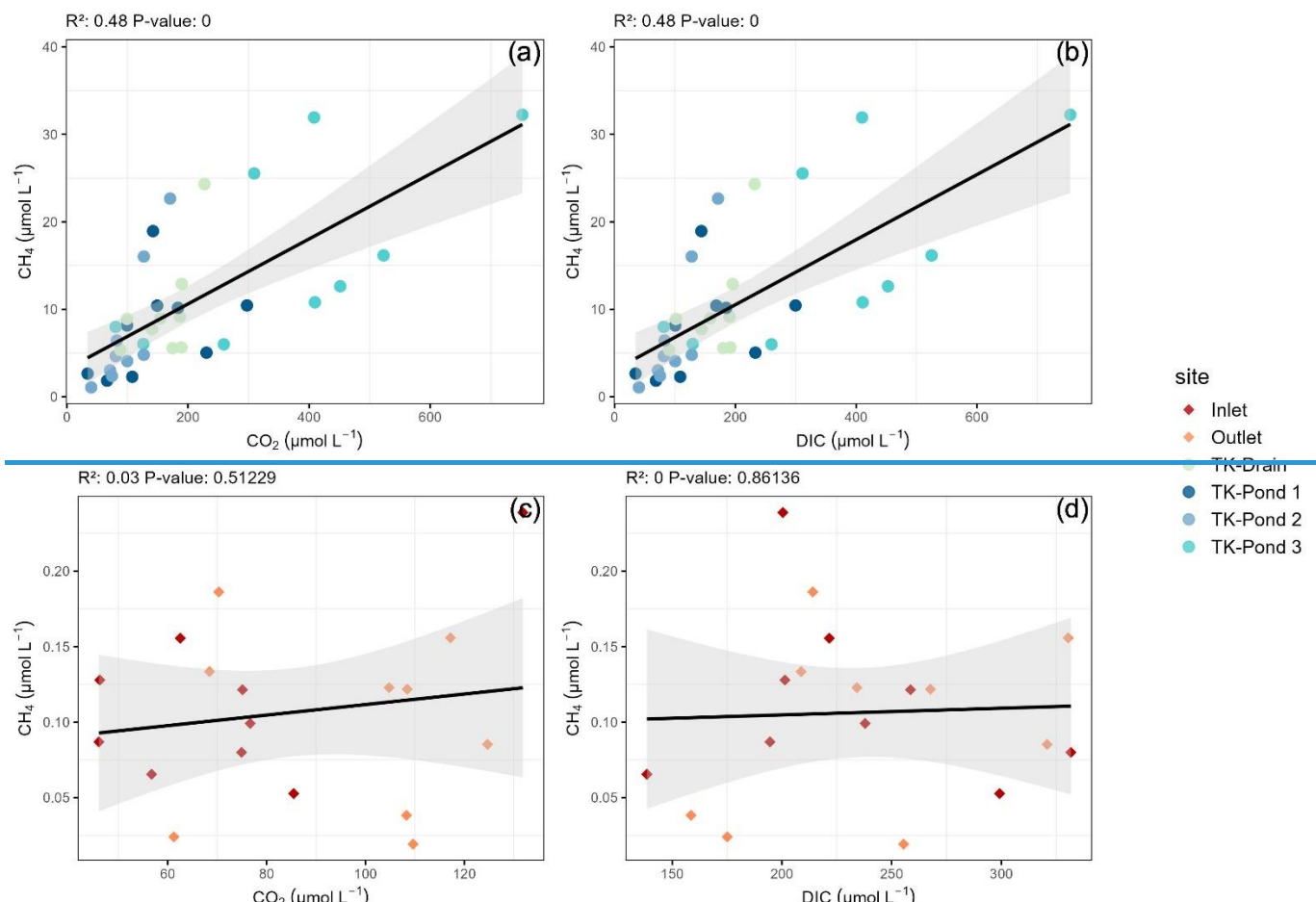
387 sources of CH₄ to the atmosphere. The lower CH₄ oversaturation in streams compared with
 388 ponds is likely related to higher CH₄ losses caused by stream turbulence and/or higher
 389 production rates of CH₄ in the thermokarst ponds (Fig. 3).



390
 391 **Figure 3 Variations in carbon dioxide (CO₂) and methane (CH₄) concentrations in relation to**
 392 **pH, DOC, and totP across sampling sites.** [Variations in dissolved CO₂ \(panels a–c\)](#) and CH₄ (panels
 393 [d–f](#)) [across sampling sites in relation to pH, DOC and totP.](#) The upper panels show the relationships
 394 [between dissolved CO₂ concentrations \(µM\) and pH \(a\), dissolved organic carbon \(DOC, mg L⁻¹\) \(b\),](#)
 395 [and total organic phosphorous \(totP, µg L⁻¹\) \(c\) in sampled water.](#) The lower panels show the
 396 [relationship between dissolved CH₄ concentrations and pH \(d\), DOC \(mg L⁻¹\) \(e\), and totP \(µg L⁻¹\) \(f\)](#)
 397 [in sampled water.](#)

398 CO₂ saturation indexes in the thermokarst waterbodies reached 5 to 20 while in the streams
 399 they ranged between 3 and 4 ([Table 3](#)). By contrast, the CO₂ evasion from the streams (e.g. 1-
 400 2 g C m⁻² day⁻¹) was higher than from the ponds (0.3-0.5 C m⁻² day⁻¹), consistent with the

401 higher turbulence in the streams, and the replenishment of CO₂ from bicarbonates from
402 groundwater in these streams, which is a geological rather than a recent source of CO₂.
403 Bicarbonates contributed about 60-70% to DIC in the wetland streams (with pH between 6.0
404 and 7.4), while bicarbonates in thermokarst water bodies were almost negligible (with pH
405 below 4.5), which is consistent with equilibrium between bicarbonates and CO₂ over these
406 pH ranges. TK-pond 3 had the lowest O₂ concentrations and the highest CH₄ and CO₂
407 concentrations of all thermokarst water bodies. Concentrations of CH₄ and CO₂DIC were
408 positively related in the thermokarst water bodies (r^2 0.48, $p < 0.0001$, F-test) but not in the
409 wetland streams (Fig. 4). Note that DIC in the streams is also not correlated with CH₄ (Fig SI
410 2).



413 **Figure 4** Relationships between CH_4 and (a) CO_2 , (b) DIC for between thermokarst waterbodies (a),
414 and (c) CO_2 , (d) DIC for Inlet and Outlet (b) sites including linear regression lines and corresponding

415 R² and p-value statistics. Note scale differences for CH₄ between thermokarst waterbodies and the
416 wetland streams.

417 The CO₂ emissions from the stream sites (Inlet and Outlet) were substantially larger than
418 those from the thermokarst waterbodies (Table 3). The mean CO₂ emission at the Inlet site
419 was 1.12 ± 0.46 g C m⁻² day⁻¹, and at the Outlet site 2.20 ± 1.15 g C m⁻² day⁻¹. These values
420 are 3 to 7 times higher than the fluxes observed from the thermokarst waterbodies, which
421 ranged from 0.30 ± 0.22 g C m⁻² day⁻¹ (TK-Pond 2) to 0.51 ± 0.28 g C m⁻² day⁻¹ (TK-Pond 3).

422 Annual CO₂ fluxes for the ice-free period, assuming negligible flux during the ice-covered
423 months, ranged between 51 g C m⁻² yr⁻¹ and 87 g C m⁻² yr⁻¹ for the thermokarst ponds, and
424 the streams ranged between 190 g C m⁻² yr⁻¹ (Inlet) and 405 g C m⁻² yr⁻¹ (Outlet).

425 **Table 3. Mean and standard deviations of dissolved gas concentrations and associated metrics**
426 **for thermokarst ponds and wetland sites across nine sampling campaigns.** Mean concentrations
427 of CO₂ (μM) and CH₄ (μM) with their respective saturation ratios, along with CO₂ emission flux (g C
428 m⁻² day⁻¹), DIC (μM), and oxygen concentrations (μM) with percent saturation. The saturation ratio is
429 defined as the concentration divided by the equilibrium concentration between the atmosphere and
430 water at the given temperature. For this study, DIC is considered the sum of dissolved CO₂ and
431 bicarbonate. Letters indicate significant differences between sites for each variable.

	CO ₂ μmol L ⁻¹	Saturation ratio CO ₂	DIC μmol L ⁻¹	CO ₂ emission g C m ⁻² day ⁻¹
TK-Pond 1	146 (82) B	7.0 (3.2) BC	149 (83) BC	0.36 (0.28) C
TK-Pond 2	97 (39) B	5.1 (2.2) BC	98 (39) C	0.30 (0.22) C
TK-Pond 3	369 (206) A	18.8 (11.3) A	371 (206) A	0.51 (0.28) C
TK-Drain	161 (45) B	8.1 (2.7) B	165 (46) BC	0.37 (0.15) C
Inlet	73 (26) B	3.1 (1.0) C	232 (59) B	1.12 (0.46) B
Outlet	97 (24) B	4.4 (1.1) BC	241 (59) B	2.20 (1.15) A

	CH ₄ μmol L ⁻¹	CH ₄ saturation ratio	O ₂	
			μmol L ⁻¹	% saturation
TK-Pond 1	7.8 (5.5) B	2 330 (1 719) B	273 (59) AB	81 (14) A
TK-Pond 2	7.2 (7.2) B	2150 (2 110) B	266 (85) AB	79 (19) A

TK-Pond 3	16.6 (10.6) A	5 109 (3 470) A	210 (89) B	61 (22) B
TK-Drain	9.8 (5.9) B	2976 (1973) B	260 (65) AB	77 (18) AB
Inlet	0.1 (0.1) C	30 (15) C	297 (59) A	81 (14) A
Outlet	0.1 (0.1) C	28 (18) C	241 (63) AB	67 (14) AB

432

433 3.3 DOM processing rates

434 Average DIC production rates in the different water bodies were highly variable (7.8 – 62.5
 435 $\mu\text{M day}^{-1}$, Table 4), but tended to be highest in the thermokarst ponds compared with the
 436 wetland streams, while the TK-drain had the lowest rates (Tukey's t-test, $p < 0.05$. The non-
 437 parametric Wilcoxon tests supported these trends, confirming minimal site-specific effects
 438 overall, with TK-Drain showing lower activity). These results reflect the in-situ processing of
 439 DOM in both thermokarst ponds and streams. The DOM mineralization rate did not vary
 440 significantly between sites and neither did the exponential decay rate kDOM (Table 4).

441 kDOM in the thermokarst ponds ranged from 4.4 yr^{-1} to 9.0 yr^{-1} (Table 4), while the [stream](#)
 442 [Outlet](#) showed higher kDOM values [from than the inlet](#) (8.8 yr^{-1} and 6.3 yr^{-1} [respectively](#)).
 443 The TK-Drain site was substantially lower (2.5 yr^{-1}).

444 **Table 4. Rates of production and decay.** DIC rates reflect DIC production. The DIC rate/DOC ratio
 445 indicates the relative efficiency of converting DOC to DIC, while kDOM indicates the exponential
 446 decay rate of DOM, showing how quickly DOM is decomposed over time. Letters indicate significant
 447 differences between sites for each variable ($p < 0.05$).

	DIC rate $\mu\text{M day}^{-1}$	DIC rate/DOC $\mu\text{mol g C}^{-1} \text{ day}^{-1}$	kDOM yr^{-1}	
TK-Pond 1	27.8 (16.5) AB	67.0 (38.9)	A	7.2 (4.2) A
TK-Pond 2	19.6 (8.8) AB	41.6 (28.7)	A	4.4 (3.1) A
TK-Pond 3	62.5 (47.0) A	83.3 (78.1)	A	9.0 (8.6) A
TK-Drain	7.8 (7.4) B	23.1 (23.4)	A	2.5 (2.5) A
Inlet	11.7 (4.5) AB	59.5 (25.8)	A	6.3 (2.8) A
Outlet	20.5 (16.7) AB	82.5 (64.7)	A	8.8 (7.0) A

448 **4. Discussion**

449 Understanding the GHG source–sink function of degrading permafrost landscapes benefits
450 from an integrated study of water chemistry and GHG fluxes, as hydrological and
451 biogeochemical processes are closely linked (Frey and McClelland, 2009; Vonk et al., 2015).
452 In particular, shifts in OM mobilization, acidity, and nutrient dynamics across different
453 thermokarst pond stages influence C cycling and GHG production. In our study area, isolated
454 thermokarst ponds and more hydrologically connected wetland streams represent contrasting
455 hydrochemical environments, with ponds reflecting strong permafrost thaw inputs and
456 streams influenced by the catchment.

457 **4.1 Water chemical contrasts between thermokarst ponds and water chemistry**

458 Thermokarst ponds and wetland streams exhibit strong contrasts in DOC concentrations and
459 acidity, with ponds showing high DOC and low pH. The inverse relationship between DOC
460 and pH ($R^2 = -0.82$, $p < 0.01$) suggests that organic acidity is a dominant driver of pH in
461 thermokarst ponds. The acidity is likely driven by the leaching of DOM from recently
462 destabilized permafrost, since the ponds are hydrologically isolated from the surrounding
463 wetland. Elevated DOM and leaching from surrounding permafrost is-are observed in other
464 thawing permafrost landscapes (Holmes et al., 2022; Ward and Cory, 2015). This is
465 consistent with the finding that TK-Pond 3—hydrologically the most isolated—has on
466 average the highest DOC (35 mg L⁻¹) and the lowest pH (4.1), indicating strong organic
467 acidity effects from destabilized permafrost and minimal exchange with the surrounding
468 wetland.

469 In contrast, wetland streams exhibit near-neutral pH values, which we attribute to
470 groundwater influence. We found systematically higher HCO₃⁻, SO₄²⁻, and SiO₂ in the
471 wetland streams than in the ponds, and also higher base cations (Table SI 3). This
472 geochemical signature is characteristic of carbonate and silicate mineral weathering occurring

473 along subsurface flow paths, which was found in several catchments at Iškorasfjellet,
474 including the Bákiljohka catchment where our study site is located (Lehmann et al. 2023).
475 Lehmann et al. (2023) documented groundwater-driven alkalinity generation linked to both
476 carbonate vein dissolution and silicate weathering and suggested that carbonate weathering
477 should be considered as a potential CO₂ source in the catchment. Groundwater effects on
478 stream waters have also been found elsewhere in permafrost landscapes (Turetsky et al.,
479 2020; Vonk et al., 2015), suggesting that CO₂ emissions from high pH-streams can be
480 replenished by geogenic rather than biogenic sources, which is important to account for in
481 GHG budgets from aquatic ecosystems.

482 Levels of totP mirrored the pattern of DOC enrichment in thermokarst ponds (30–70 µg L⁻¹),
483 demonstrating that P in these nutrient-poor ponds is primarily organically bound (Frey et al.,
484 2007). In addition to DOC, permafrost thaw releases organic forms of P that can affect
485 downstream nutrient dynamics and carbon cycling (in 't Zandt et al., 2020). In contrast, the
486 lower DOC and totP found in the wetland streams reflected the influence from upstream
487 catchment, including groundwater inputs. The higher POC concentrations in the thermokarst
488 ponds (1.2–3.4 mg L⁻¹ L) compared to wetland streams (0.4–0.6 mg L⁻¹ L) further supports
489 that thermokarst ponds are hotspots for OM destabilization, whereas wetland streams are
490 more influenced by lateral transport and groundwater (Olefeldt and Roulet, 2014).

491 The hydrochemical contrasts between thermokarst ponds and wetland streams at Iškoras,
492 shaped by differences in DOC concentrations, acidity, and groundwater influence, are key
493 drivers of spatial variation in GHG production and emissions across the landscape. Given the
494 strong controls of DOC and pH on CH₄ dynamics (Shirokova et al., 2012; Segers, 1998),
495 these patterns provide important context for understanding permafrost–C feedbacks.
496 production and, also g. Comment on: contrasts in pH: in ponds, primary driver of pH appears
497 to be organic acidity while in streams (can be supported with reference), groundwater

498 influences dominate wetlands (can be supported with references that GW is enriched with
499 carbonates, SO₄, SiO₂ from weathering).. Illustrates that the ponds are hydrologically
500 isolated from the wetland, with the channel as an intermediate.
501 The inverse relationship between DOC and pH points towards organic acidity as a strong
502 driver of pH. Additionally, the near to neutral pH in the wetland streams is consistent with
503 groundwater influences from the catchment, which also would explain the elevated SiO₂ and
504 SO₄ concentrations. A limited set of water samples were analysed for base cations (Table SI
505 3), confirming that these were highest in the wetland streams.

506 Low pH and elevated totP concentrations are commonly related to increased DOM
507 concentrations (Holmes et al., 2022; Ward and Cory, 2015), which could originate from
508 destabilized permafrost (Turetsky et al., 2020).

509 4.12 Thermokarst ponds as hotspots of methane emissions
510 Thermokarst ponds in Iškoras display CH₄ saturation indexes of 2300 to 5000 (Table 3),
511 which is among the highest values reported in the literature for natural waterbodies,
512 particularly in northern permafrost regions. These findings align with Shirokova et al. (2012)
513 and Matveev et al. (2018) who documented saturation indexes of 50 to 5000 in Siberian
514 thermokarst depressions, and of 5 to 50 in subarctic lithalsa lakes, respectively. Such high
515 CH₄ concentrations in these poorly connected, small, and relatively protected water bodies
516 are consistent with the established inverse relationship between CH₄ concentrations and water
517 body size, hydrological connectivity, and turbulence exposure (Abnizova et al., 2012;
518 Kankaala et al., 2013; Polishchuk et al., 2018).

519 At Iškoras, the smallest pond, TK-Pond 3, exhibited the highest CH₄ oversaturation, in
520 combination with the highest DOC, totP, and lowest pH values mentioned earlier. This could
521 be explained by creation of anaerobic sediments and C-rich conditions, and low pH, by
522 permafrost thaw and limited hydrological connectivity, that in concert enhance CH₄

523 production. The high DOM, originating from destabilized permafrost (Turetsky et al., 2020)
524 is usually associated with low pH and elevated totP (Holmes et al., 2022; Ward and Cory,
525 2015. Thus, CH₄ oversaturation in thermokarst ponds could be related to particularly high
526 DOC availability, and to acidic conditions that limit CH₄ oxidation (Wik et al., 2016).

527 Despite the presence of dissolved O₂ in thermokarst ponds, they remained highly
528 oversaturated in CH₄. CH₄ production is known to occur mainly in anoxic sediments
529 (Bastviken et al., 2004; Clayer et al., 2016; Wik et al., 2016), from where CH₄ is
530 subsequently transported to overlying water. The microbial activity responsible for CH₄
531 production may be enhanced by the release of previously frozen OM from ongoing
532 thermokarst development (Crevecoeur et al., 2017), as recently observed in laboratory
533 incubations with inundated peat from the Iškoras site (Kjær, 2024).

534 As thermokarst ponds evolve into wetlands, CH₄ emission patterns may shift due to changes
535 in hydrological connectivity and biogeochemical cycling. Pirk et al. (2024) used a space-for-
536 time substitution to highlight that the transition from thermokarst ponds to wetlands at
537 Iškoras involves significant changes in GHG fluxes, finding that the degradation of palsas to
538 thermokarst ponds led to a 17-fold increase in local GHG forcing, primarily driven by CH₄
539 and CO₂ emissions. This is partly because thermokarst ponds, being spatially isolated, create
540 localized CH₄ emission hotspots (Elder et al., 2021). Wetlands, with their larger spatial extent
541 and greater hydrological connectivity, promote slower organic matter mineralization, which
542 can reduce CO₂ emissions and increase carbon uptake (Pirk, et al., 2024). Although wetlands
543 continue to emit CH₄, these emissions become more diffuse rather than concentrated at
544 hotspots. At the same time, wetlands can act as net carbon sinks, as CO₂ uptake through plant
545 productivity and organic matter accumulation may offset greenhouse gas emissions
546 (Heiskanen et al., 2023; de Wit et al., 2015). This transition represents a fundamental shift
547 from localized, CH₄-dominated GHG emissions in thermokarst ponds to a more spatially

548 diffuse CH₄ emissions in wetlands, where increased CO₂ uptake and OM accumulation can
549 contribute to a net C sink (Turetsky et al., 2020).

550 Similarly, at Iškoras, the smallest pond exhibited the highest CH₄ oversaturation, in
551 combination with the highest DOC, totP, and lowest pH values, likely linked to
552 destabilization of thawing permafrost combined with limited hydrological connectivity. Low
553 pH and elevated totP concentrations are commonly related to increased DOM concentrations
554 (Holmes et al., 2022; Ward and Cory, 2015), which could originate from destabilized
555 permafrost (Turetsky et al., 2020).

556 Thermokarst ponds were highly oversaturated in CH₄ despite the presence of dissolved O₂.
557 CH₄ production is known to occur mainly in anoxic sediments (Bastviken et al., 2004; Clayer
558 et al., 2016; Wik et al., 2016), from where CH₄ is subsequently transported to overlying
559 water. The microbial activity responsible for CH₄ production may be enhanced by fresh OM
560 input from ongoing thermokarst development (Crevecoeur et al., 2017), as recently observed
561 in laboratory incubations with recently inundated peat material from the Iškoras site (Kjær,
562 2024).

563 1.1.1 – 4.2 Impact of thawing peat plateaus on water chemistry
564 The transition of permafrost underlain peat plateaus to thermokarst ponds and further to
565 wetlands can markedly shift the landscape scale GHG dynamics as permafrost continues to
566 thaw (Hugelius et al., 2020; Sannel and Kuhry, 2011). Thermokarst ponds are localized CH₄
567 hotspots; however, as these systems transition into wetlands, emissions patterns change due
568 to altered hydrology and biogeochemistry (Holmes et al., 2022; Peura et al., 2019). In
569 wetlands, persistent inundation creates anoxic conditions favourable for methanogenesis,
570 often leading to significant CH₄ emissions (Cui et al., 2024). Pirk et al. (2024) demonstrated
571 that fens at Iškoras, as an example of such inundated wetland systems, emit large amounts of
572 CH₄, particularly where fresh OC is available from peat decomposition from degrading palsas

573 edges. Similarly, Turetsky et al. (2020) noted that newly formed wetlands, arising from
574 permafrost thaw become additional CH₄ sources due to labile OC availability.

575 Holmes et al. (2022) observed that inundation in permafrost landscapes increases CH₄
576 emissions because of waterlogged conditions that limit oxygen diffusion and enhance
577 anaerobic decomposition. Additionally, Kjær et al. (2024) highlighted that recently thawed
578 permafrost peat in wetland systems, including peat from Iškoras, features a high CH₄
579 production potential due to the presence of labile C and methanogenic microbial
580 communities.

581 Unlike thermokarst ponds, which are spatially limited, wetlands have a wider spatial extent.
582 The carbon balance in wetlands depends not only on CH₄ fluxes but also on changes in CO₂
583 dynamics as organic matter mineralization occurs under waterlogged conditions (Turetsky et
584 al., 2020). In this context, the transition from thermokarst ponds to wetlands represents a shift
585 from localized emissions of both CH₄ and CO₂ to more spatially homogenous CH₄ emissions,
586 while CO₂ is sequestered (Pirk et al., 2024).

587 Although a focus on vertical fluxes dominates many studies, lateral DOC fluxes also play a
588 role in carbon dynamics in permafrost affected systems. Wetland and peatland ecosystems
589 exhibit high rates of lateral DOC export due to hydrological connectivity (Tank et al., 2018).
590 Beekebanze et al. (2022) reported that lateral fluxes, though smaller in magnitude compared
591 to vertical fluxes, are essential in carbon budgets, potentially contributing to carbon loss
592 especially during peak runoff events. These lateral DOC fluxes transport carbon from soils to
593 aquatic systems, where it may later contribute to downstream GHG emissions or C
594 sequestration. The potential for fens and wetlands to transition into significant GHG
595 contributors and increased hydrological connectivity leading to greater potential lateral C

596 ~~fluxes highlights the need for integrated C budget models that capture the evolving landscape~~
597 ~~dynamics in permafrost regions.~~

598 4.3 Carbon dioxide dynamics ~~in thermokarst water bodies~~

599 Both thermokarst ponds and streams in Iškoras are oversaturated with CO₂ (Table 3), a
600 common feature of Arctic and subarctic aquatic systems (Allesson et al., 2022; Bastviken et
601 al., 2004). However, the mechanisms driving CO₂ fluxes differ between ponds and streams.
602 In ponds, despite high CO₂ concentrations, CO₂ release is lower than in streams and likely
603 limited by the lack of turbulence. ~~By In~~ contrast, streams exhibit enhanced CO₂ fluxes likely
604 due to high turbulence and carbonate inputs ~~from groundwater~~, as described ~~in section 4.1.~~
605 ~~Others have also found that groundwater influences can contribute both who emphasized the~~
606 ~~role of groundwater-derived bicarbonate and dissolved CO₂ s into~~ ~~sustaining stream~~ CO₂
607 fluxes ~~in Arctic streams~~ (Lehmann et al., 2023; Duvert et al., 2018; Winterdahl et al., 2016).
608 ~~This highlights that groundwater contributions of bicarbonate and dissolved CO₂ must be~~
609 ~~accounted for when interpreting stream CO₂ fluxes, as ignoring these inputs could lead to~~
610 ~~overestimating the importance of recently mineralized DOM or newly produced CO₂ from~~
611 ~~thermokarst ponds.~~

612 Quantitatively, CO₂ efflux from streams at Iškoras averages 0.4 g C m⁻² day⁻¹ (Table 3),
613 aligning closely with values observed in Siberian permafrost streams (0.3–0.5 g C m⁻² day⁻¹;
614 (Shirokova et al., 2012)). This flux ~~reflects is consistent with~~ the ~~combined influence of~~
615 ~~turbulent flow and groundwater inputs enriched in DIC, consistent with earlier findings of~~
616 ~~mineral weathering contributions to DIC at Iškorasfjellet (Lehmann et al., 2023). significant~~
617 ~~contribution of turbulent flow and bicarbonate rich groundwater inputs, processes shown to~~
618 ~~facilitate CO₂ release. These findings complement observations from other regions, where~~
619 ~~turbulence and bicarbonate supply are key drivers of CO₂ release in streams~~ (Lundin et al.,
620 2013; Raymond et al., 2013). Streams ~~likely~~ benefit from continuous replenishment of CO₂

621 from bicarbonates, which account for 60–70% of [the DIC pool](#) in [these environments](#)
622 [boreal to Arctic streams and rivers](#) (Wallin et al., 2018; Zolkos and Tank, 2020).

623 In contrast, CO₂ emissions from ponds at Iškoras are notably low (Table 3), similar to
624 findings of Campeau and Del Giorgio (2014), attributed to the ponds' high DOC-to-
625 bicarbonate ratios, which restrict bicarbonate formation and subsequent CO₂ production
626 (Abnizova et al., 2012; Bastviken et al., 2004). The limited water mixing in ponds further
627 diminishes CO₂ flux due to low gas exchange rates compared to streams. However, DIC
628 production rates in ponds (26.7–35.7 $\mu\text{M day}^{-1}$) remain sufficient to sustain CO₂ effluxes of
629 5–10 mol C $\text{m}^{-2} \text{ year}^{-1}$, consistent with findings by (Shirokova et al., 2012), who linked DIC
630 production directly to DOC concentrations in Arctic aquatic systems. [These DIC production](#)
631 [rates, together with our measured kDOM values \(4.4–9.0 \$\text{yr}^{-1}\$; Table 4\), appear relatively](#)
632 [elevated when compared to the mean DOC degradation rate for lakes \(\$2.5 \pm 4.0 \text{ yr}^{-1}\$ \), based](#)
633 [on converted daily rates reported by Catalán et al. \(2016\).](#)

634 High CO₂ evasion from lower-order streams is caused by high flow velocities and associated
635 turbulence causing high gas exchanges (Schelker et al., 2016). These drivers likely explain
636 the relatively higher CO₂ efflux from Iškoras streams compared to ponds. [We suggest that](#)
637 [mineralization of DOM, influenced by DOM lability, pH and nutrients, plays a critical role](#)
638 [for CO₂ emissions of the thermokarst ponds.](#) High molecular-weight DOM, as indicated by
639 low sUVA and SAR values, can [be more resistant to microbial processing than low-](#)
640 [molecular-weight DOM](#), thereby slowing DOM decay rates (Shirokova et al., 2019). Ward
641 and Cory (2015) noted that DOM from thawing permafrost, while less aromatic and more
642 labile compared to active layer DOM, may become limited by environmental factors such as
643 pH and nutrient availability, resulting in lower mineralization rates. The acidic conditions in
644 ponds could shift microbial communities and affect activity (Vigneron et al., 2019), a factor
645 that can further limit CO₂ fluxes from ponds in addition to the low gas exchange rate.

646 In summary, the higher CO₂ fluxes observed in streams at Iškoras are likely driven by the
647 combined effects of turbulent flow, groundwater-derived DIC, and mineral weathering
648 inputs, bicarbonate input, and mineral weathering, whereas lower emissions from ponds are
649 shaped by organic acidity, limited hydrological connectivity, and lack of turbulence limited
650 surface exchange. These dynamics emphasize the need to account for the interaction of
651 hydrological and chemical factors when assessing the fate of destabilized OM in water bodies
652 C fluxes in permafrost-impacted regions.

653 4.4 Climate feedback implications
654 The distinct roles of CH₄ and CO₂ in the Iškoras landscape underscore their unique climate
655 feedback potentials. The transition from thermokarst ponds to wetlands modifies the overall
656 GHG footprint of the peatland-wetland continuum, balancing the loss of localized CH₄
657 emission hotspots with the emergence of sustained, long-term CH₄ emissions from wetlands,
658 while the fate of organic matter currently stored in permafrost remains uncertain. At the same
659 time, CO₂ fluxes from the streams and rivers may increase due to enhanced hydrological
660 connectivity and increased organic matter input (Zolkos et al., 2019), in agreement with the
661 results of our study. At Iškoras, the small spatial extent of the permafrost area limits its
662 overall impact on the catchment-scale GHG source–sink function. However, in landscapes
663 where peat plateaus occupy a larger area, such transitions may have more significant
664 consequences at the regional scale. These findings reflect the complex interplay of ecological
665 and hydrological factors shaping GHG emissions in permafrost landscapes. Turetsky et al.
666 (2020) and Pirk et al. (2024) both emphasized the need for further research on the
667 spatiotemporal variability of these factors, particularly during thaw cycles, as shifts in
668 hydrological connectivity, OM transport, and microbial activity can significantly influence
669 the GHG emissions and permafrost-C feedbacks. Improving our understanding of these

670 [dynamics is t](#)[essential for refin](#)[inge](#) predictions of permafrost-C feedbacks [in a changing](#)
671 [climate.](#)

672 5. Conclusions

673 This study highlights the distinct biogeochemical roles of thermokarst ponds and wetland
674 streams in a landscape of sporadic permafrost in subarctic Norway. Thermokarst ponds at the
675 Iškoras site, characterized by low pH, high organic acidity, and elevated DOC concentrations,
676 are currently hotspots for CH₄ emissions, with stable DOM lability driving sustained carbon
677 processing. In contrast, wetland streams exhibit higher CO₂ fluxes, largely driven by
678 turbulence and bicarbonate replenishment from groundwater. Despite similarities in DOM
679 mineralization rates between ponds and streams, environmental constraints, such as pH,
680 microbial community composition, and hydrodynamic mixing, are likely controls of the
681 observed differences in GHG fluxes. As thermokarst ponds transition into wetlands, they will
682 no longer function as hotspots for CH₄ emissions. Instead, CH₄ emissions are likely to
683 increase across the entire landscape, as sustained waterlogging promotes elevated CH₄
684 production. These ecological shifts, coupled with lateral DOC losses from peat plateaus,
685 highlight the importance of hydrological connectivity in linking terrestrial and aquatic C
686 dynamics. Such transitions emphasize the need for integrated C budget models that account
687 for the evolving contributions of small aquatic systems to regional and global C cycles.
688 Future research should prioritize direct measurements of CH₄ fluxes, microbial community
689 contributions to DOM decomposition under varying environmental constraints, and the
690 temporal variability of gas production and emissions. Additionally, exploring seasonal
691 dynamics, lateral carbon transport, and hydrological processes will provide critical insights
692 into C cycling. Investigating catchment-scale signals, such as DOC concentrations across
693 entire river systems and their links to permafrost contributions, can further advance our
694 understanding of landscape-level processes. By addressing these questions, we can better

695 predict the trajectory of permafrost-impacted landscapes and their feedbacks to the global C
696 cycle in a warming climate.

697 **6. Data availability**

698 All data [presented in this manuscript are publicly available at](#)
699 <https://doi.org/10.4211/hs.41faf3d6c3f245259ea820740291789c> supporting this study will be
700 ~~made available on a permanent repository upon acceptance.~~

701 **7. Author contributions**

702 JKK and HDW conceptualized the study. JKK, HDW and FC participated in data collection.
703 JKK, FC, HDW and PD conducted the experiments and performed data analysis. JKK, HDW
704 and FC created the figures. JKK and HDW drafted the initial manuscript, and HDW, FC, SW
705 and PD revised and edited the final version.

706 **8. Competing interests**

707 The authors declare that they have no conflict of interest.

708 **Acknowledgements**

709 NIVA core funding (Research Council of Norway, contract nr 342628/L10) Global Change at
710 Northern Latitudes, BIOGOV project (Research Council of Norway, project nr 323945), Uta
711 Brandt, Hanna Lee, Inge Althuizen, Emelie Forsman

712

9. References

Abnizova, A., Siemens, J., Langer, M., and Boike, J.: Small ponds with major impact: The relevance of ponds and lakes in permafrost landscapes to carbon dioxide emissions, *Global Biogeochemical Cycles*, 26, 2, <https://doi.org/10.1029/2011GB004237>, 2012.

Aleweli, C., Giesler, R., Klaminder, J., Leifeld, J., and Rollog, M.: Stable carbon isotopes as indicators for environmental change in palsal peats, *Biogeosciences*, 8, 1769–1778, <https://doi.org/10.5194/bg-8-1769-2011>, 2011.

Allesson, L., Valiente, N., Dorsch, P., Andersen, T., Eiler, A., and Hessen, D.O.: Drivers and variability of CO₂:O₂ saturation along a gradient from boreal to Arctic lakes, *Sci. Rep.*, 12, 18989, <https://doi.org/10.1038/s41598-022-23705-9>, 2022.

[Aresenault, J., Talbot, J., Brown, L.E., Holden, J., Martinez-Cruz, K., Sepulveda-Juaregui, A., Swindles, G.T., Wauthy, M., Lapierre, J.: Biogeochemical distinctiveness of peatland ponds, thermokarst waterbodies, and lakes, *Geophysical Research Letters*, 49, e2021GL097492, <https://doi.org/10.1029/2021GL097492>, 2022.](#)

Bansal, S., Post van der Burg, M., Fern, R.R., Jones, J.W., Lo, R., McKenna, O.P., Tangen, B.A., Zhang, Z., and Gleason, R.A.: Large increases in methane emissions expected from North America's largest wetland complex, *Sci. Adv.*, 9, eade1112, <https://doi.org/10.1126/sciadv.ade1112>, 2023.

Bastviken, D., Cole, J., Pace, M., and Tranvik, L.: Methane emissions from lakes: Dependence of lake characteristics, two regional assessments, and a global estimate, *Global Biogeochemical Cycles*, 18, <https://doi.org/10.1029/2004GB002238>, 2004.

Bastviken, D., Sundgren, I., Natchimuthu, S., Reyier, H., and Gålfalk, M.: Cost-efficient approaches to measure carbon dioxide (CO₂) fluxes and concentrations in terrestrial and aquatic environments using mini loggers, *Biogeosciences*, 12, 3849–3859, <https://doi.org/10.5194/bg-12-3849-2015>, 2015.

Beckebanze, L., Runkle, B.R.K., Walz, J., Wille, C., Holl, D., Helbig, M., Boike, J., Sachs, T., and Kutzbach, L.: Lateral carbon export has low impact on the net ecosystem carbon balance of a polygonal tundra catchment, *Biogeosciences*, 19, 3863–3876, <https://doi.org/10.5194/bg-19-3863-2022>, 2022.

Borge, A.F., Westermann, S., Solheim, I., and Etzelmüller, B.: Strong degradation of palsas and peat plateaus in northern Norway during the last 60 years, *Cryosphere*, 11, 1–16, <https://doi.org/10.5194/tc-11-1-2017>, 2017.

Boudreau, B.P., and Ruddick, B.R.: On a reactive continuum representation of organic matter diagenesis, *Am. J. Sci.*, 291, 507–538, 1991.

Campeau, A., and Del Giorgio, P.A.: Patterns in CH₄ and CO₂ concentrations across boreal rivers: Major drivers and implications for fluvial greenhouse emissions under climate change scenarios, *Glob. Chang. Biol.*, 20, 1075–1088, <https://doi.org/10.1111/gcb.12479>, 2014.

Catalán, N., Marcé, R., Kothawala, D.N., and Tranvik, L.J.: Organic carbon decomposition rates controlled by water retention time across inland waters, *Nat. Geosci.*, 9, 501–504, <https://doi.org/10.1038/ngeo2720>, 2016.

Clayer, F., Gobeil, C., and Tessier, A.: Rates and pathways of sedimentary organic matter mineralization in two basins of a boreal lake: Emphasis on methanogenesis and methanotrophy, *Limnol. Oceanogr.*, 61, S1, <https://doi.org/10.1002/lno.10323>, 2016.

Crevecoeur, S., Vincent, W.F., Comte, J., Matveev, A., and Lovejoy, C.: Diversity and potential activity of methanotrophs in high methane-emitting permafrost thaw ponds, *PLoS ONE*, 12, e0188223, <https://doi.org/10.1371/journal.pone.0188223>, 2017.

Cui, S., Liu, P., Guo, H., Nielsen, C.K., Pullens, J.W.M., Chen, Q., Pugliese, L., and Wu, S.: Wetland hydrological dynamics and methane emissions, *Commun. Earth Environ.*, 5, 1, <https://doi.org/10.1038/s43247-024-01635-w>, 2024.

[de Wit, H.A., Austnes, K., Hylen, G., and Dalsgaard, L.: A Carbon Balance of Norway: Terrestrial and Aquatic Carbon Fluxes, *Biogeochemistry*, 123, 317–342, <https://doi.org/10.1007/s10533-014-0060-5>, 2015.](#)

765 [Duvert, C., Butman, D.E., Marx, A., Ribolzi, O., et al.: CO₂ Evasion Along Streams Driven by](#)
 766 [Groundwater Inputs and Geomorphic Controls, Nat. Geosci., 11, 813–818,](#)
 767 [https://doi.org/10.1038/s41561-018-0245-y, 2018.](https://doi.org/10.1038/s41561-018-0245-y)

768 [Elder, C.D., Thompson, D.R., Thorpe, A.K., et al.: Characterizing Methane Emission Hotspots From](#)
 769 [Thawing Permafrost, Global Biogeochem. Cycles, 35, e2020GB006922,](#)
 770 [https://doi.org/10.1029/2020GB006922, 2021.](https://doi.org/10.1029/2020GB006922)

771 [Frey, K.E., McClelland, J.W., Holmes, R.M., and Smith, L.C.: Impacts of Climate Warming and](#)
 772 [Permafrost Thaw on the Riverine Transport of Nitrogen and Phosphorus to the Kara Sea, J.](#)
 773 [Geophys. Res.-Biogeosci., 112, G04S58, https://doi.org/10.1029/2006JG000369, 2007.](#)

774 [Frey, K. E., and McClelland, J. W.: Impacts of permafrost degradation on arctic river](#)
 775 [biogeochemistry, Hydrol. Process., 23, 169–182, https://doi.org/10.1002/hyp.7196, 2009.](#)

776 Gisnås, K., Etzelmüller, B., Lussana, C., Hjort, J., Sannel, A.B.K., Isaksen, K., Westermann, S.,
 777 Kuhry, P., Christiansen, H.H., Frampton, A., and Åkerman, J.: Permafrost Map for Norway,
 778 Sweden, and Finland, Permafrost Periglac. Process., 28, 359–378,
 779 https://doi.org/10.1002/ppp.1922, 2017.

780 [Gundersen, C.B., Velasco, M.T., Velle, G., Rogora, M., Hawley, K.L., Fölster, J., Nygren, I., Vogt,](#)
 781 [R.D., Kolado, A., Pasztaleniec, A. and Bryntesen, T.: ICP Waters Programme Manual.](#)
 782 [NIVA-rapport. https://hdl.handle.net/11250/3178113, 2025.](#)

783 [Heiskanen, L., Tuovinen, J.-P., Vekuri, H., Räsänen, A., Virtanen, T., Juutinen, S., Lohila, A.,](#)
 784 [Mikola, J., and Aurela, M.: Meteorological responses of carbon dioxide and methane fluxes in](#)
 785 [the terrestrial and aquatic ecosystems of a subarctic landscape, Biogeosciences, 20, 545–572,](#)
 786 [In 't Zandt, M.H., Liebner, S., and Welte, C.U.: Roles of Thermokarst Lakes in a Warming World,](https://doi.org/10.5194/bg-20-545-2023, 2023.</p>
<p>787 Holgerson, M.A. and Raymond, P.A.: Large contribution to inland water CO₂ and CH₄ emissions

 788 from very small ponds, Nat. Geosci., 9, 222–226, https://doi.org/10.1038/ngeo2654, 2016.</p>
<p>789 Holmes, M.E., Crill, P.M., Burnett, W.C., McCalley, C.K., Wilson, R.M., Frolking, S., Chang, K.Y.,

 790 Riley, W.J., Varner, R.K., Hodgkins, S.B., McNichol, A.P., Saleska, S.R., Rich, V.I., and

 791 Chanton, J.P.: Carbon Accumulation, Flux, and Fate in Stordalen Mire, a Permafrost Peatland

 792 in Transition, Glob. Biogeochem. Cycles, 36, https://doi.org/10.1029/2021GB007113, 2022.</p>
<p>793 Hugelius, G., Loisel, J., Chadburn, S., Jackson, R.B., Jones, M., Macdonald, G., Marushchak, M.,

 794 Olefeldt, D., Packalen, M., Siewert, M.B., Treat, C., Turetsky, M., Voigt, C., and Yu, Z.:

 795 Large stocks of peatland carbon and nitrogen are vulnerable to permafrost thaw, Proc. Natl.

 796 Acad. Sci. U.S.A., 117, 20438–20446, https://doi.org/10.1073/pnas.1916387117, 2020.</p>
<p>797 Hugelius, G., Strauss, J., Zubrzycki, S., Harden, J.W., Schuur, E.A.G., Ping, C.L., Schirrmeister, L.,

 798 Grosse, G., Michaelson, G.J., Koven, C.D., O'Donnell, J.A., Elberling, B., Mishra, U., Camill,

 799 P., Yu, Z., Palmtag, J., and Kuhry, P.: Estimated stocks of circumpolar permafrost carbon

 800 with quantified uncertainty ranges and identified data gaps, Biogeosciences, 11, 6573–6593,

 801 https://doi.org/10.5194/bg-11-6573-2014, 2014.</p>
<p>802 <a href=)
 803 [Trends Microbiol., 28, 769–779, https://doi.org/10.1016/j.tim.2020.04.002, 2020.](#)

804 Kankaala, P., Huotari, J., Tulonen, T., and Ojala, A.: Lake-size dependent physical forcing drives
 805 carbon dioxide and methane effluxes from lakes in a boreal landscape, Limnol. Oceanogr.,
 806 58, 1915–1930, https://doi.org/10.4319/lo.2013.58.6.1915, 2013.

807 Kjellman, S.E., Axelsson, P.E., Etzelmüller, B., Westermann, S., and Sannel, A.B.K.: Holocene
 808 development of subarctic permafrost peatlands in Finnmark, northern Norway, Holocene, 28,
 809 1855–1869, https://doi.org/10.1177/0959683618798126, 2018.

810 Kjær, S.T., Westermann, S., Nedkvitne, N., and Dörsch, P.: Carbon degradation and mobilisation
 811 potentials of thawing permafrost peatlands in northern Norway inferred from laboratory
 812 incubations, Biogeosciences, 21, 4723–4737, https://doi.org/10.5194/bg-21-4723-2024, 2024.

813 Krutskikh, N., Ryazantsev, P., Ignashov, P., and Kabonen, A.: The Spatial Analysis of Vegetation
 814 Cover and Permafrost Degradation for a Subarctic Palsa Mire Based on UAS
 815 Photogrammetry and GPR Data in the Kola Peninsula, Remote Sens., 15, 1896,
 816 https://doi.org/10.3390/rs15071896, 2023.

817 Krüger, J.P., Conen, F., Leifeld, J., and Alewell, C.: Palsa Uplift Identified by Stable Isotope Depth
 818 Profiles and Relation of δ¹⁵N to C/N Ratio, Permafrost Periglac. Process., 28, 485–492,
 819 https://doi.org/10.1002/ppp.1936, 2017.

820 Kuhn, M., Lundin, E.J., Giesler, R., Johansson, M., and Karlsson, J.: Emissions from thaw ponds
821 largely offset the carbon sink of northern permafrost wetlands, *Sci. Rep.*, 8,
822 <https://doi.org/10.1038/s41598-018-27770-x>, 2018.

823 Laurion, I., Massicotte, P., Mazoyer, F., Negandhi, K., and Mladenov, N.: Weak mineralization
824 despite strong processing of dissolved organic matter in Eastern Arctic tundra ponds, *Limnol.*
825 *Oceanogr.*, 66, <https://doi.org/10.1002/lno.11634>, 2020.

826 [Lehmann, N., Lantuit, H., Böttcher, M.E., and Hartmann, J.: Alkalinity Generation from Carbonate](#)
827 [Weathering in a Silicate-Dominated Headwater Catchment at Iskorasfjellet, Northern](#)
828 [Norway, Biogeosciences, 20, 3459–3478, https://doi.org/10.5194/bg-20-3459-2023, 2023.](#)

829 Leppiniemi, O., Karjalainen, O., Aalto, J., Luoto, M., and Hjort, J.: Environmental spaces for palsas
830 and peat plateaus are disappearing at a circumpolar scale, *Cryosphere*, 17, 3157–3176,
831 <https://doi.org/10.5194/tc-17-3157-2023>, 2023.

832 Lundin, E.J., Giesler, R., Persson, A., Thompson, M.S., and Karlsson, J.: Integrating carbon emissions
833 from lakes and streams in a subarctic catchment, *J. Geophys. Res.-Biogeosci.*, 118, 1200–
834 1207, <https://doi.org/10.1002/jgrg.20092>, 2013.

835 Martin, L.C.P., Nitzbon, J., Scheer, J., Aas, K.S., Eiken, T., Langer, M., Filhol, S., Etzelmüller, B.,
836 and Westermann, S.: Lateral thermokarst patterns in permafrost peat plateaus in northern
837 Norway, *Cryosphere*, 15, 3423–3442, <https://doi.org/10.5194/tc-15-3423-2021>, 2021.

838 Martin, L.C.P., Nitzbon, J., Aas, K.S., Etzelmüller, B., Kristiansen, H., and Westermann, S.: Stability
839 Conditions of Peat Plateaus and Palsas in Northern Norway, *J. Geophys. Res.-Earth Surf.*,
840 124, 705–719, <https://doi.org/10.1029/2018JF004945>, 2019.

841 Matveev, A., Laurion, I., and Vincent, W.F.: Methane and carbon dioxide emissions from thermokarst
842 lakes on mineral soils, *Arct. Sci.*, 4, 584–604, <https://doi.org/10.1139/as-2017-0047>, 2018.

843 [Meredith, M., Sommerkorn, M., Cassotta, S., Derksen, C., Ekaykin, A., Hollowed, A., Kofinas, G.,](#)
844 [Mackintosh, A., Melbourne-Thomas, J., Muelbert, M. M. C., Ottersen, G., Pritchard, H., and](#)
845 [Schuur, E. A. G.: Polar Regions, in: IPCC Special Report on the Ocean and Cryosphere in a](#)
846 [Changing Climate, United States National Marine Fisheries Service, United States National](#)
847 [Oceanic and Atmospheric Administration Office of Oceanic and Atmospheric Research, and](#)
848 [Intergovernmental Panel on Climate Change \(IPCC\),](#)
849 [https://repository.library.noaa.gov/view/noaa/27411, 2019.](https://repository.library.noaa.gov/view/noaa/27411)

850 Mostovaya, A., Hawkes, J.A., Dittmar, T., and Tranvik, L.J.: Molecular Determinants of Dissolved
851 Organic Matter Reactivity in Lake Water, *Frontiers in Earth Science*, 5,
852 <https://doi.org/10.3389/feart.2017.00106>, 2017.

853 Muster, S., Riley, W.J., Roth, K., Langer, M., Cresto Aleina, F., Koven, C.D., Lange, S., Bartsch, A.,
854 Grosse, G., Wilson, C.J., Jones, B.M., and Boike, J.: Size Distributions of Arctic Waterbodies
855 Reveal Consistent Relations in Their Statistical Moments in Space and Time, *Frontiers in*
856 *Earth Science*, 7, <https://doi.org/10.3389/feart.2019.00005>, 2019.

857 Muster, S., Roth, K., Langer, M., Lange, S., Cresto Aleina, F., Bartsch, A., Morgenstern, A., Grosse,
858 G., Jones, B., Sannel, A.B.K., Sjöberg, Y., Günther, F., Andresen, C., Veremeeva, A.,
859 Lindgren, P.R., Bouchard, F., Lara, M.J., Fortier, D., Charbonneau, S., Virtanen, T.A.,
860 Hugelius, G., Palmtag, J., Siewert, M.B., Riley, W.J., Koven, C.D., and Boike, J.: PeRL: A
861 Circum-Arctic Permafrost Region Pond and Lake Database, *Earth System Science Data*, 9,
862 317–348, <https://doi.org/10.5194/essd-9-317-2017>, 2017.

863 Olefeldt, D., Heffernan, L., Jones, M.C., Sannel, A.B.K., Treat, C.C., Turetsky, M.R.: Permafrost
864 Thaw in Northern Peatlands: Rapid Changes in Ecosystem and Landscape Functions. In:
865 Canadell, J.G., Jackson, R.B. (eds) *Ecosystem Collapse and Climate Change. Ecological*
866 *Studies*, vol 241. Springer, Cham. https://doi.org/10.1007/978-3-030-71330-0_3, 2021.

867 [Olefeldt, D. and Roulet, N.T.: Permafrost Conditions in Peatlands Regulate Magnitude, Timing, and](#)
868 [Chemical Composition of Catchment Dissolved Organic Carbon Export, Glob. Change Biol.](#)
869 [20, 3122–3136, https://doi.org/10.1111/gcb.12607, 2014.](#)

870 Payette, S., Delwaide, A., Caccianiga, M., and Beauchemin, M.: Accelerated Thawing of Subarctic
871 Peatland Permafrost over the Last 50 Years, *Geophysical Research Letters*, 31, 18,
872 <https://doi.org/10.1029/2004GL020358>, 2004.

873 Peura, S., Wauthy, M., Simone, D., Eiler, A., Einarsdóttir, K., Rautio, M., and Bertilsson, S.:
874 Ontogenetic Succession of Thermokarst Thaw Ponds Is Linked to Dissolved Organic Matter

875 Quality and Microbial Degradation Potential, Limnology and Oceanography, 65(S1),
 876 <https://doi.org/10.1002/lno.11349>, 2019.

877 Pirk, N., Aalstad, K., Mannerfelt, E.S., Clayer, F., de Wit, H., Christiansen, C.T., Althuizen, I., Lee,
 878 H., and Westermann, S.: Disaggregating the Carbon Exchange of Degrading Permafrost
 879 Peatlands Using Bayesian Deep Learning, *Geophysical Research Letters*, 51, 10,
 880 <https://doi.org/10.1029/2024GL109283>, 2024.

881 Polishchuk, Y.M., Bogdanov, A.N., Muratov, I.N., Polishchuk, V.Y., Lim, A., Manasypov, R.M.,
 882 Shirokova, L.S., and Pokrovsky, O.S.: Minor Contribution of Small Thaw Ponds to the Pools
 883 of Carbon and Methane in the Inland Waters of the Permafrost-Affected Part of the Western
 884 Siberian Lowland, *Environmental Research Letters*, 13, 4, <https://doi.org/10.1088/1748-9326/aab046>, 2018.

885 Raymond, P.A., Hartmann, J., Lauerwald, R., Sobek, S., McDonald, C., Hoover, M., Butman, D.,
 886 Striegl, R., Mayorga, E., Humborg, C., Kortelainen, P., Dürr, H., Meybeck, M., Ciais, P., and
 887 Guth, P.: Global Carbon Dioxide Emissions from Inland Waters, *Nature*, 503, 7476, 355–359,
 888 <https://doi.org/10.1038/nature12760>, 2013.

889 R Core Team: R: A Language and Environment for Statistical Computing, R Foundation for
 890 Statistical Computing, Vienna, Austria, <https://www.R-project.org/>, 2021.

891 Sannel, A.B.K., and Kuhry, P.: Warming-Induced Destabilization of Peat Plateau/Thermokarst Lake
 892 Complexes, *Journal of Geophysical Research: Biogeosciences*, 116, G3,
 893 <https://doi.org/10.1029/2010JG001635>, 2011.

894 Schelker, J., Singer, G.A., Ulseth, A.J., Hengsberger, S., and Battin, T.J.: CO₂ Evasion from a Steep,
 895 High Gradient Stream Network: Importance of Seasonal and Diurnal Variation in Aquatic
 896 pCO₂ and Gas Transfer, *Limnology and Oceanography*, 61, 5, 1826–1838,
 897 <https://doi.org/10.1002/lno.10339>, 2016.

898 Schuur, E.A.G., Bockheim, J., Canadell, J.G., Euskirchen, E., Field, C.B., Goryachkin, S.V.,
 899 Hagemann, S., Kuhry, P., Lafleur, P.M., Lee, H., Mazhitova, G., Nelson, F.E., Rinke, A.,
 900 Romanovsky, V.E., Shiklomanov, N., Tarnocai, C., Venevsky, S., Vogel, J.G., and Zimov,
 901 S.A.: Vulnerability of Permafrost Carbon to Climate Change: Implications for the Global
 902 Carbon Cycle, *Bioscience*, 58, 8, 701–714, <https://doi.org/10.1641/B580807>, 2008.

903 Schuur, E.A.G., McGuire, A.D., Schädel, C., Grosse, G., Harden, J.W., Hayes, D.J., Hugelius, G.,
 904 Koven, C.D., Kuhry, P., Lawrence, D.M., Natali, S.M., Olefeldt, D., Romanovsky, V.E.,
 905 Schaefer, K., Turetsky, M.R., Treat, C.C., and Vonk, J.E.: Climate Change and the Permafrost
 906 Carbon Feedback, *Nature*, 520, 7546, 171–179, <https://doi.org/10.1038/nature14338>, 2015.

907 [Schuur, E.A., Abbott, B.W., Commane, R., Ernakovich, J., Euskirchen, E., Hugelius, G., Grosse, G., Jones, M., Koven, C., Leshyk, V. and Lawrence, D.: Permafrost and climate change: Carbon cycle feedbacks from the warming Arctic. Annual Review of Environment and Resources, 47\(1\), pp.343-371, https://doi.org/10.1146/annurev-environ-012220-011847, 2022.](https://doi.org/10.1146/annurev-environ-012220-011847)

908 [Segers, R.: Methane Production and Methane Consumption: A Review of Processes Underlying Wetland Methane Fluxes, Biogeochemistry, 41, 23–51, https://doi.org/10.1023/A:1005929032764, 1998.](https://doi.org/10.1023/A:1005929032764)

909 SeNorge: Norges vassdrags- og energidirektorat, Norsk: <https://www.senorge.no/>, last access 22
 910 November 2024.

911 Shirokova, L. S., Chupakov, A. V., Zabelina, S. A., Neverova, N. V., Payandi-Rolland, D.,
 912 Causserand, C., Karlsson, J., and Pokrovsky, O. S.: Humic surface waters of frozen peat bogs
 913 (permafrost zone) are highly resistant to bio- and photodegradation, *Biogeosciences*, 16(12),
 914 2511–2526, <https://doi.org/10.5194/bg-16-2511-2019>, 2019.

915 Shirokova, L. S., Pokrovsky, O. S., Kirpotin, S. N., Desmukh, C., Pokrovsky, B. G., Audry, S., and
 916 Viers, J.: Biogeochemistry of organic carbon, CO₂, CH₄, and trace elements in thermokarst
 917 water bodies in discontinuous permafrost zones of Western Siberia, *Biogeochemistry*, 113(1–
 918 3), 573–593, <https://doi.org/10.1007/s10533-012-9790-4>, 2012.

919 Sim, T. G., Swindles, G. T., Morris, P. J., Baird, A. J., Cooper, C. L., Gallego-Sala, A. V., Charman,
 920 D. J., Roland, T. P., Borken, W., Mullan, D. J., Aquino-López, M. A., and Gałka, M.:
 921 Divergent responses of permafrost peatlands to recent climate change, *Environ. Res. Lett.*,
 922 16(3), 035003, <https://doi.org/10.1088/1748-9326/abe00b>, 2021.

929 Sollid, J. L., Andersen, S., Hamre, N., Kjeldsen, O., Salvigsen, O., Sturød, S., Tveitå, T., and
930 Wilhelmsen, A.: Deglaciation of Finnmark, North Norway, *Norsk Geografisk Tidsskr.*, 27(4),
931 233–325, <https://doi.org/10.1080/00291957308551960>, 1973.

932 [Strauss, J., Fuchs, M., Hugelius, G., Miesner, F., Nitze, I., Opfergelt, S., Schuur, E., Treat, C.,](#)
933 [Turetsky, M., Yang, Y., and Grosse, G.: Organic matter storage and vulnerability in the](#)
934 [permafrost domain, in: Encyclopedia of Quaternary Science \(Third edition\), edited by: Elias,](#)
935 [S., Elsevier, 399–410, https://doi.org/10.1016/B978-0-323-99931-1.00164-1, 2025.](#)

936 Stumm, W. and Morgan, J.J.: *Aquatic chemistry: chemical equilibria and rates in natural waters*. John
937 Wiley & Sons, 2013.

938 Swindles, G. T., Morris, P. J., Mullan, D., Watson, E. J., Turner, T. E., Roland, T. P., Amesbury, M.
939 J., Kokfelt, U., Schonning, K., Pratte, S., Gallego-Sala, A., Charman, D. J., Sanderson, N.,
940 Garneau, M., Carrivick, J. L., Woulds, C., Holden, J., Parry, L., and Galloway, J. M.: The
941 long-term fate of permafrost peatlands under rapid climate warming, *Sci. Rep.*, 5, 17951,
942 <https://doi.org/10.1038/srep17951>, 2015.

943 Tank, S. E., Fellman, J. B., Hood, E., and Kritzberg, E. S.: Beyond respiration: Controls on lateral
944 carbon fluxes across the terrestrial–aquatic interface, *Limnol. Oceanogr. Lett.*, 3(3), 76–88,
945 <https://doi.org/10.1002/lol2.10068>, 2018.

946 Thrane, J.-E., de Wit, H., Blakseth, T.A., Skancke, L.B. and Garmo, Ø.A.: Correcting for bias in
947 freshwater total nitrogen concentrations obtained with a modified standard (NS4743) method.
948 NIVA-rapport, 2020.

949 Turetsky, M. R., Abbott, B. W., Jones, M. C., Anthony, K. W., Olefeldt, D., Schuur, E. A. G., Grosse,
950 G., Kuhry, P., Hugelius, G., Koven, C., Lawrence, D. M., Gibson, C., Sannel, A. B. K., and
951 McGuire, A. D.: Carbon release through abrupt permafrost thaw, *Nat. Geosci.*, 13(2), 138–
952 143, <https://doi.org/10.1038/s41561-019-0526-0>, 2020.

953 Valiente, N., Eiler, A., Allesson, L., Andersen, T., Clayer, F., Crapart, C., Dörsch, P., Fontaine, L.,
954 Heuschele, J., Vogt, R. D., Wei, J., de Wit, H. A., and Hessen, D. O.: Catchment properties as
955 predictors of greenhouse gas concentrations across a gradient of boreal lakes, *Front. Environ.*
956 Sci., 10, <https://doi.org/10.3389/fenvs.2022.880619>, 2022.

957 Verdonen, M., Störmer, A., Lotsari, E., Korpelainen, P., Burkhard, B., Colpaert, A., and Kumpula, T.:
958 Permafrost degradation at two monitored palsa mires in north-west Finland, *The Cryosphere*,
959 17, 1803–1819, <https://doi.org/10.5194/tc-17-1803-2023>, 2023.

960 Vigneron, A., Cruaud, P., Bhiry, N., Lovejoy, C., and Vincent, W. F.: Microbial community structure
961 and methane cycling potential along a thermokarst pond-peatland continuum,
962 *Microorganisms*, 7, 1–16, <https://doi.org/10.3390/microorganisms7110486>, 2019.

963 Vogt, R.D. and Skancke, L.B.: *Overvåking av langtransportert forurenset luft og nedbør. Årsrapport–*
964 *Vannkjemiske effekter 2021*. NIVA report 7778-2022; Miljødirektoratet report 2347-2022,
965 2022.

966 Vonk, J. E., Tank, S. E., Bowden, W. B., Laurion, I., Vincent, W. F., Alekseychik, P., Amyot, M.,
967 Billet, M. F., Canário, J., Cory, R. M., Deshpande, B. N., Helbig, M., Jammet, M., Karlsson,
968 J., Larouche, J., MacMillan, G., Rautio, M., Walter Anthony, K. M., and Wickland, K. P.:
969 Reviews and syntheses: Effects of permafrost thaw on Arctic aquatic ecosystems,
970 *Biogeosciences*, 12, 7129–7167, <https://doi.org/10.5194/bg-12-7129-2015>, 2015.

971 Vähäalto, A. V., Aarnos, H., and Mäntyniemi, S.: Biodegradability continuum and biodegradation
972 kinetics of natural organic matter described by the beta distribution, *Biogeochemistry*, 100,
973 227–240, <https://doi.org/10.1007/s10533-010-9419-4>, 2010.

974 Wallin, M. B., Campeau, A., Audet, J., Bastviken, D., Bishop, K., Kokic, J., Laudon, H., Lundin, E.,
975 Löfgren, S., Natchimuthu, S., Sobek, S., Teutschbein, C., Weyhenmeyer, G. A., and Grabs,
976 T.: Carbon dioxide and methane emissions of Swedish low-order streams: A national estimate
977 and lessons learnt from more than a decade of observations, *Limnol. Oceanogr. Lett.*, 3, 156–
978 167, <https://doi.org/10.1002/lol2.10061>, 2018.

979 Walter, K. M., Chanton, J. P., Chapin, F. S. III, Schuur, E. A. G., and Zimov, S. A.: Methane
980 production and bubble emissions from arctic lakes: Isotopic implications for source pathways
981 and ages, *J. Geophys. Res.-Biogeosci.*, 113, G03001, <https://doi.org/10.1029/2007JG000569>,
982 2008.

983 Walter, K. M., Zimov, S. A., Chanton, J. P., Verbyla, D., and Chapin, F. S.: Methane bubbling from
984 Siberian thaw lakes as a positive feedback to climate warming, *Nature*, 443, 71–75,
985 <https://doi.org/10.1038/nature05040>, 2006.

986 Ward, C. P., and Cory, R. M.: Chemical composition of dissolved organic matter draining permafrost
987 soils, *Geochim. Cosmochim. Acta*, 167, 63–79, <https://doi.org/10.1016/j.gca.2015.07.001>,
988 2015.

989 Westrich, J. T., and Berner, R. A.: The role of sedimentary organic matter in bacterial sulfate
990 reduction: The G model tested, *Limnol. Oceanogr.*, 29, 236–249,
991 <https://doi.org/10.4319/lo.1984.29.2.0236>, 1984.

992 Wickham, H.: *ggplot2: Elegant Graphics for Data Analysis*, Springer-Verlag New York, ISBN 978-3-
993 319-24277-4, <https://ggplot2.tidyverse.org>, 2016.

994 Wik, M., Varner, R. K., Anthony, K. W., MacIntyre, S., and Bastviken, D.: Climate-sensitive northern
995 lakes and ponds are critical components of methane release, *Nat. Geosci.*, 9, 99–105,
996 <https://doi.org/10.1038/ngeo2578>, 2016.

997 Wilhelm, E., Battino, R., and Wilcock, R. J.: Low-pressure solubility of gases in liquid water, *Chem.*
998 *Rev.*, 77, 219–262, <https://doi.org/10.1021/cr60306a003>, 1977.

999 Winterdahl, M., Wallin, M. B., Karlsen, R. H., Laudon, H., Öquist, M., and Lyon, S. W.: Decoupling
1000 of carbon dioxide and dissolved organic carbon in boreal headwater streams, *Journal of*
1001 *Geophysical Research: Biogeosciences*, 121, 2630–2651,
1002 <https://doi.org/10.1002/2016JG003420>, 2016.

1003 Yang, H., Andersen, T., Dörsch, P., Tominaga, K., Thrane, J.-E., and Hessen, D. O.: Greenhouse gas
1004 metabolism in Nordic boreal lakes, *Biogeochemistry*, 126, 211–225,
1005 <https://doi.org/10.1007/s10533-015-0154-8>, 2015.

1006 Zimov, S. A., Davydov, S. P., Zimova, G. M., Davydova, A. I., Schuur, E. A. G., Dutta, K., and
1007 Chapin, F. S. III: Permafrost carbon: Stock and decomposability of a globally significant
1008 carbon pool, *Geophys. Res. Lett.*, 33, L20502, <https://doi.org/10.1029/2006GL027484>, 2006.

1009 Zolkos, S., and Tank, S. E.: Experimental evidence that permafrost thaw history and mineral
1010 composition shape abiotic carbon cycling in thermokarst-affected stream networks, *Front.*
1011 *Earth Sci.*, 8, 1–11, <https://doi.org/10.3389/feart.2020.00152>, 2020.

1012 Zolkos, S., Tank, S. E., Striegl, R. G., and Kokelj, S. V.: Thermokarst effects on carbon dioxide and
1013 methane fluxes in streams on the Peel Plateau (NWT, Canada), *J. Geophys. Res.-Biogeosci.*,
1014 124, 1781–1798, <https://doi.org/10.1029/2019JG005038>, 2019.

1015 Zolkos, S., Tank, S. E., and Kokelj, S. V.: Mineral weathering and the permafrost carbon-climate
1016 feedback, *Geophysical Research Letters*, 45, 9623–9632,
1017 <https://doi.org/10.1029/2018GL078748>, 2018.

1018 Åberg, J., and Wallin, M. B.: Evaluating a fast headspace method for measuring DIC and subsequent
1019 calculation of $p\text{CO}_2$ in freshwater systems, *Inland Waters*, 4, 157–166,
1020 <https://doi.org/10.5268/IW-4.2.694>, 2014.